Iron catalysts for the selective production of ethene and propene by means of the Fischer-Tropsch synthesis

IRON CATALYSTS FOR THE SELECTIVE PRODUCTION OF ETHENE AND PROPENE BY MEANS OF THE FISCHER-TROPSCH SYNTHESIS

E.PH.KIEFFER

IRON CATALYSTS FOR THE SELECTIVE PRODUCTION OF ETHENE AND PROPENE BY MEANS OF THE FISCHER-TROPSCH SYNTHESIS

PROEFSCHRIFT

TER VERKRIJGING VAN DE GRAAD VAN DOCTOR IN DE TECHNISCHE WETENSCHAPPEN AAN DE TECHNISCHE HOGESCHOOL EINDHOVEN, OP GEZAG VAN DE RECTOR MAGNIFICUS, PROF. IR. J. ERKELENS, VOOR EEN COMMISSIE AANGEWEZEN DOOR HET COLLEGE VAN DEKANEN IN HET OPENBAAR TE VERDEDIGEN OP DINSDAG 17 MAART 1981 TE 16.00 UUR

DOOR

EDUARD PHILIP KIEFFER

GEBOREN TE ARNHEM

DRUK WIBRO HELMOND

Dit proefschrift is goedgekeurd
door de promotoren

Prof.drs. H.S. van der Baan
en
Prof.ir. J.W. Geus

Aan mijn ouders

Aan Caroline

This investigation was supported by The Netherlands Foundation for Chemical Research (SON) with the financial aid from The Netherlands Organization for advancement of Pure Research (ZWO).

CONTENTS

CHAPTER 1

Introduction

1.1. COAL AS CHEMICAL FEEDSTOCK

With a tenfold increase in output in less than thirty years, the chemical industry has evolved as one of the most important industrial sectors. An assured continuation of the feedstock supply for this industry is hence of great economical importance. The present dependency of the chemical industry on oil and gas is a weak point in that respect, but that need not be a permanent situation. In principle, any carbon source, from wastes to agricultural products, can be used as a raw material. But coal, with extensive reserves distributed all over the world, will certainly be a very important energy-and-chemical-feedstock.

1.1.1. Organic chemicals from coal

Nowadays an important part of the organic chemicals is manufactured from crude oil in conjunction with the production of fuel. If we change from oil and gas to coal as a primary feedstock for fuels and chemicals, no great change in this relation is to be expected. Pyrolysis- (Char Oil Energy Development) and direct liquefaction-processes (Solvent Refined Coal, H-Coal, Synthoil, Exxon Donor Solvent) under development, convert coal to a product that is roughly comparable to crude oil and consists mainly of branched and naphtenic hydrocarbons. Due to their structure, these products are not directly suitable as a cracking feedstock for the manufacture of the most

important organic chemicals, the light olefins as ethene and propene. However, the product can be upgraded with convensional oil-based techniques to fuel fractions and the major aromatics, as benzene, toluene and xylene (BTX).

Indirect liquefaction processes (Fischer-Tropsch, Mobil) decompose the coal by gasification. The subsequent conversion of the resulting synthesis gas yields a product, that is not only an excellent naphta, but can also have a high content of light olefines.

1.1.2. Economics of coal-based processes

In principle, direct liquefaction processes offer better economics than the processes based on synthesis gas conversion. The reason for this disadvantage is the lower thermal efficiency of the indirect liquefaction processes, due to the strongly endothermic coal gasification. Comparison of the economics of the H-Coal process and the Mobil process[1] shows that the first is more advantageous than the latter for the production of gasoline.

When the attention is focussed on the economical production of light olefines, the synthesis gas conversion processes offer better perspectives. At present the developments of the Mobil process mainly aim at the conversion of synthesis gas to high octane gasoline, but there are also possibilities to make this process more selective towards light olefines[2].

Undoubtedly, the Fischer-Tropsch synthesis is a promising alternative for the production of light olefines. The SYNTHOL process of Sasol (South-Africa) already yields 27 weight percent C_2-C_3 olefines as a primary product. Another 17 percent can be produced by cracking the 33 percent product gasoline[3]. This does not mean that the production of light olefines by the Synthol process is already economically feasible. Improvement of the selectivity towards C_2-C_3 olefines is required for a profitable Fischer-Tropsch synthesis.

1.2. THE FISCHER-TROPSCH PROCESS

For the Fischer-Tropsch process the reactant gases are produced by steam-oxygen gasification of coal. The product from the gasifier

is cleaned and shifted to the desired H_2-to-CO ratio via the watergas shift reaction. Thereafter carbon monoxide is catalytically hydrogenated to mainly hydrocarbons and oxygenates. The reactions involved in the synthesis of hydrocarbons read:

$3\ C + 3\ H_2O = 3\ CO + 3\ H_2$	gasification
$CO + H_2O = CO_2 + H_2$	watergas shift
$2\ CO + 4\ H_2 = 2\text{-}CH_2\text{-} + 2\ H_2O$	synthesis
$3\ C + 2\ H_2O = CO_2 + 2\text{-}CH_2\text{-}$	overall process

Within limits the product composition can be shifted in the desired direction by adjusting the process conditions and selecting the proper catalyst (Co, Ni, Fe, Ru).

The following paragraphs will concentrate on some features of the Fischer-Tropsch synthesis and especially on iron as a catalyst.

1.2.1. Activity of the catalyst

Fischer-Tropsch catalysts show poor activity in the synthesis under atmospheric pressure. Turnover numbers ranging from 0.33 molecules/site/second for ruthenium to 0.03 for cobalt are usually reported[4].

The rate of the synthesis on iron catalysts is controlled by the temperature and by the partial pressures of hydrogen, carbon monoxide and water. A kinetic expression, suggested by several authors[5-8] reads:

$$r = \frac{k(H_2)}{1 + b(H_2O)/(CO)}$$

At low conversions the rate is controlled by the temperature and by the hydrogen pressure[9]:

$$r = k(H_2)$$

with: k,b = temperature dependent factors

(X) = pressure of component X

r = reaction rate

Apart from their influence on the reaction rate, temperature and pressure have a marked influence on the product distribution[5].

1.2.2. Product selectivity

With respect to iron catalysts, the average molecular weight of the hydrocarbons decreases with temperature, and the mean molecular weight of the product increases with pressure up to 3 MPa[5].

The distribution of the synthesis product can generally be described by a mechanism in which the chains grow by stepwise addition of identical single carbon units, in which the probability of propagation (α) and termination ($1-\alpha$) remains independent of the chain length. Friedel and Anderson[10] have developed the statistics to describe the product distribution of the Fischer-Tropsch synthesis by this mechanism. Henrici-Olivé and Olivé[11,12] demonstrated that the same statistics are involved in the description of the radical polymerization of vinylmonomers (Schulz (1935)[13]) and the linear polycondensation of polymers (Flory (1936)[14]). Nowadays such a product distribution, that is characterized by one parameter, α, is called a Schulz-Flory distribution. The result of the statistical approach of the product distribution is denoted in equation (1.1).

$$\ln(w_n/n) = \ln\left(w_o(1-\alpha)^2/\alpha\right) + n\ln\alpha \qquad (1.1)$$

in which:

w_n = weight of the product containing n carbon atoms

w_o = weight of the total hydrocarbon product

α = probability of propagation

The Schulz-Flory distribution is often graphically represented by plotting $\ln(w_n/n)$ as a function of n; the value of α is calculated from the slope of the Schulz-Flory plot.

The maximum ethylene selectivity that can be obtained thus equals the total C_2 selectivity. For any catalyst that obeys the Schulz-Flory distribution this maximum ethylene selectivity is 30 weight percent

Figure 1.1 Schulz-Flory type plot of the required and the obtained selectivities.

Curve a (●) : economically profitable Fischer-Tropsch synthesis[15].

Curve b (△,□): Büssemeier patent[16]: iron catalyst (CO/H_2 = 1).

Curve c (▽) : Rautavuoma[17]: cobalt catalyst (CO/H_2 = 3).

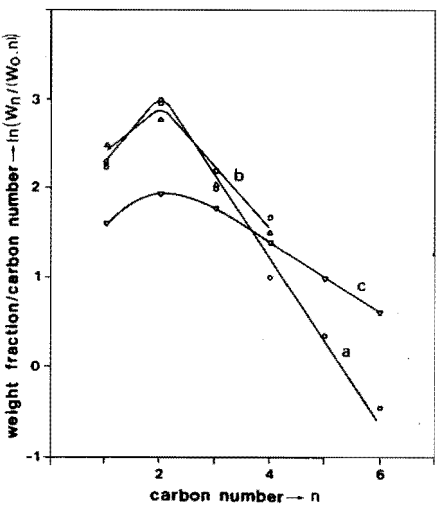

of the total hydrocarbon product at a value of α = 0.33. The combined production of small olefines (C_2 + C_3) at the same value of α is 45 weight percent, provided that no saturated products are formed. An economical evaluation of the profitability of the synthesis[15] (calculation basis: 1974) reveals that about 55 weight percent of the product must consist of light olefines to obtain an economically viable process. The value of 55 percent light olefine selectivity is not constant in time. When a revaluation is made of investment and production costs and of profits, on early 1980 basis, the required selectivity has dropped to about 48 weight percent of light olefines. However, a catalyst following the Schulz-Flory distribution will not give a profitable process. We consequently need a product mix that deviates from the Schulz-Flory distribution, e.g. the one shown in figure 1.1 (curve a) (with 55% by weight of ethene and propene). A number of recent publications has shown that this selectivity picture

is not purely hypothetical. The selectivity of the process depicted in curve b is claimed in a patent by Büssemeier et al.[16], and also in the open literature Rautavuoma[17] shows that depending on the process conditions, an undershoot in the methane production can be obtained.

Apart from the chain-length distribution, the ratio of olefines to paraffines is of utmost importance. Under normal reaction conditions α-olefines are thermodynamically unstable with respect to paraffines and β-olefines. Because α-olefines are present in appreciable quantities, they have to be primary reaction products. Secundairy reactions, as hydrogenation and isomerisation, transform α-olefines to paraffines and β-olefines. The extent of these reactions depends on the space velocity and the selectivity of the catalyst[18]. The temperature has no drastic effect on the olefine content of the product[5]. In general, the ability of the olefines to be hydrogenated decrease with their molecular weight. To our disadvantage ethylene is found to be an exception to this rule[19].

1.2.3. Deactivation and desintegration

Although the selectivity pattern of iron catalysts is favourable for the synthesis of light olefine, iron shows a number of complicating features that other active metals do not exhibit. Unlike nickel and cobalt, iron catalysts tend to form oxides and carbides upon exposure to synthesis gas. These phase transformations deactivate the catalyst to some degree and change the product selectivity. The formation of carbides and oxides, as well as carbon deposition at high temperatures by the Boudouard reaction, can moreover cause desintegration of the catalyst particles to a very fine powder that, in fixed bed reactors, leads to a high pressure drop over the catalyst bed and eventually to complete plugging of the reactor[7].

1.3. AIM AND OUTLINE OF THE PRESENT INVESTIGATION

In this chapter a number of problems are introduced that have to be overcome before a profitable Fischer-Tropsch process is viable. In the first place, the catalyst has to be modified in such a way that the carbon monoxide and hydrogen are converted in a profitable

product mix. Secondly, the catalyst must have a long life. Formation of carbon during the synthesis shortens the life of the catalyst and has to be prevented. Furthermore, a higher synthesis activity would be favourable if the synthesis activity of the catalyst is increased.

The main aim of the investigation has been to establish the factors that determine the behavior of the catalyst with respect to its selectivity towards light olefines, its synthesis activity, and its activity for carbon deposition, and to find a catalyst that meets the demands formulated above.

In chapter 2 a description is given of the reactor systems that are used in the experiments.

The results of the search for a catalyst that selectively converts synthesis gas to light olefines are described in chapter 3. The build up of carbonaceous material in the catalyst during the synthesis is also discussed in this chapter, because the formation of these species is directly related to the activity and selectivity of the catalyst.

It was found that carbon deposited onto the catalyst affects the activity differently. The first carbon affects the activity appreciably whereas carbon deposition in later stages does not markedly influence the activity. The types of carbonaceous species that influence the synthesis activity and selectivity of the iron catalyst are therefore subjected to a more extensive study in chapter 4. The different species are distinguished by their reactivity towards hydrogen.

In chapter 5 the transient method is applied to find whether the low turnover frequency on iron catalysts can be explained by a low rate constant for chain propagation, as has been published with ruthenium.

In chapter 6 an attempt will be made to give a consistent description of the factors that determine the behavior of the iron catalyst. The description will be based on the literature and the results presented in chapters 3, 4 and 5.

REFERENCES

1. Harney, B.M., Mills, G.A., Joseph, L.M., Symposium on Advances in Fischer-Tropsch Chemistry, Div. Petroleum Chemistry, Inc. Am. Chem. Soc., Anaheim Meeting 573 (1978)
2. Rao, V.U.S., Gormley, R.J., Hydrocarbon Processing 59, (11), 138 (1980)
3. Frohning, C.D., Cornils, B., Hydrocarbon Processing 53, (11), 143 (1974)
4. Vannice, M.A., J. Catal. 37, 449 (1975)
5. Anderson, R.B., Catalysis, Vol. IV, P.H. Emmett, Ed., Reinhold, New York, N.Y. (1956)
6. Hall, W.K., Kokes, R.J., Emmett, P.H., J. Am. Chem. Soc. 82, 1027 (1960)
7. Dry, M.E., Ind. Eng. Chem.-Prod. Res. Dev. 15, 282 (1976)
8. Atwood, H.E., Bennett, C.O., Ind. Eng. Chem.-Proc. Des. Dev. 18, 163 (1979)
9. Dry, M.E., Shingles, T., Boshoff, L.J., J. Catal. 25, 99 (1972)
10. Friedel, R.A., Anderson, R.B., J. Am. Chem. Soc. 72, 1212, 2307 (1950)
11. Henrici-Olivé, G., Olivé, S., Angew. Chem. 88, 144 (1976)
12. Henrici-Olivé, G., Olivé, S., J. Catal. 60, 481 (1979)
13. Schulz, G.V., Z. Phys. Chem. B-29, 299 (1935); B-30, 375 (1935); B-32, 27 (1936)
14. Flory, P.J., J. Am. Chem. Soc. 58, 1877 (1936)
15. The Stage and Development Possibilities of the Fischer-Tropsch Synthesis for the Production of Primary Chemicals and Feedstock, Final Report, Bundes Ministerium für Forschung und Technologie (1977)
16. Ruhrchemie A.G., Deutsches Offenlegungsschrift 2518964 (1976)
17. Rautavuoma, A.O.I., Thesis, TH Eindhoven, 50 (1979)
18. Pichler, H., Schulz, H., Hojabri, F., Brennstoff Chemie 45, 215 (1964)
19. Pichler, H., Schulz, H., Chem.-Ing.-Tech. 42, 1162 (1970)

CHAPTER 2

Reactor systems

2.1. INTRODUCTION

In chapter 3 the activity and the selectivity of different iron catalysts will be discussed. To be able to compare the synthesis performances of the different catalysts straightforwardly, the tests are performed in an isothermal plug flow reactor. The reaction conditions are chosen in such a way that the requirements for differential operation are always fulfilled. A number of stability tests, as described in chapter 3, are performed in a gas recirculation reactor.

In chapter 4 the different types of surface and subsurface carbonaceous deposits are discussed. The deposits are formed upon interaction of carbon monoxide or synthesis gas with the iron catalyst. Because it is necessary in this study to be able to expose the catalyst to limited amounts of reactant gas, the measurements are performed in a reactor system that can be operated as a pulse as well as a continuous flow reactor.

In chapter 5 the transient behavior of the iron catalyst is discussed. The experiments are carried out in a pulse flow reactor system, which is carefully constructed so that it is possible to obtain a well shaped step function in the concentration to the reactor. This system is also operated under differential conditions.

2.2. *REACTOR SYSTEM I: THE CONTINUOUS FLOW FIXED BED REACTOR SYSTEM (figure 2.1)*

A glass fixed bed reactor with an inside diameter of 6 mm is surrounded by an electric oven. The oven temperature is regulated by an Eurotherm thyristor controller and a chromel-alumel thermocouple. The gases hydrogen (Hoekloos, purity 99.9%), carbon monoxide (Matheson, c.p., purity 99.5%) and helium (Hoekloos, purity 99,995%) are separately purified by a reduced copper catalyst (BASF R3-11, B.T.S.) at 425 K and by a molecular sieve (5A, Union Carbide) at 300 K. The product gas samples are analysed by three gaschromatographs. On the first two (Philips-Pye, FID) the analysis of hydrocarbons from C_1 to C_6 is achieved. The third gaschromatograph, equipped with a katharometer (Philips-Pye) is used to separate carbon monoxide and water. The detection of water during the experiment is inaccurate, because of peak broadening and the low quantity of water produced.

Figure 2.1. The continuous flow fixed bed reactor system (I).

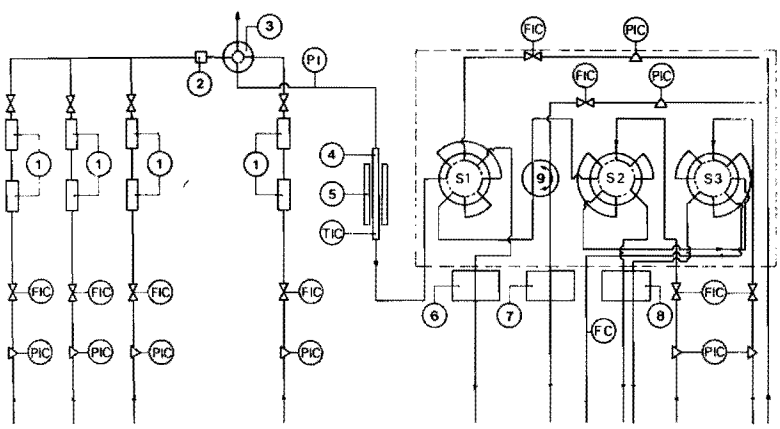

1. columns filled with B.T.S. catalyst and molecular sieve
2. van Dyke mixer
3. 4-way valve
4. reactor tube
5. furnace
6. GLC 1 with F.I.D.
7. GLC 2 with F.I.D.
8. GLC 3 with katharometer S1, S2 8-way gas sampling valves S3 4-way disc gas sampling valve
9. 4-way disc gas sampling valve

2.3. *REACTOR SYSTEM II: THE COMBINED PULSE AND CONTINUOUS FLOW FIXED BED REACTOR SYSTEM (figure 2.2)*

A stainless steel fixed bed reactor with an inside diameter of 3.6 mm is placed in a chromatograph oven (Philips-Pye), of which the heating rate can be programmed linearly. The temperature in the oven and in the catalyst bed is registrated with chromel-alumel thermocouples. The separate purification of the gases helium (Hoekloos, purity 99.995%), carbon monoxide (Matheson, c.p., purity 99.5%) and hydrogen (Hoekloos, purity 99.9%) is for each gas performed by a reduced copper catalyst (BASF R3-11, B.T.S.) and a molecular sieve (5A, Union carbide). The reactants and products are analysed by gaschromatography. The analysing unit is composed of a Porapak Q column and a connection in series of a katharometer (Hewlett-Packard) and a flame ionisation detector (Philips-Pye).

Figure 2.2. The combined pulse and continuous flow fixed bed reactor system (II).

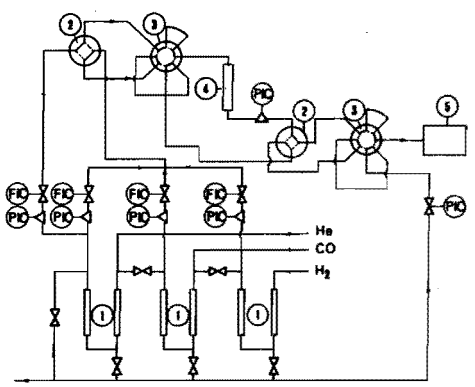

1. columns filled with B.T.S. catalyst and molecular sieve
2. 4-way valve
3. 8-way gas sampling valve
4. reactor
5. gaschromatograph with F.I.D. and katharometer

When the system is in pulse operation, helium is used as the carrier gas. Aliquots of 0.25 cm^3 (N.T.P.) can be injected into the carrier gas by a Becker eight way valve. The carrier gas transports the pulse to the reactor. During the pulse flow operation the reactor exit is connected on line with the analysing unit. The reactor pressure is 0.3 MPa at a carrier gas flow rate of 0.75 cm^3/s (N.T.P.).

During continuous flow operation the reactant is continuously fed to the reactor. The effluent gas stream from the reactor bypasses the gaschromatograph and samples for analysis are taken from the effluent stream. In continuous flow operation the system operates between 0.1 and 0.4 MPa.

2.4. REACTOR SYSTEM III: THE COMBINED PLUG FLOW AND CONTINUOUS RECIRCULATION REACTOR SYSTEM

The reactor system is developed for kinetic measurements. Since this system has only been used for the catalyst stability tests discussed in this thesis, the description of this reactor system will be short. A complete description and characterisation of the apparatus will be published elsewhere, together with the results of the kinetic study.

Figure 2.3. The combined plug flow and continuous recirculation reactor (III).

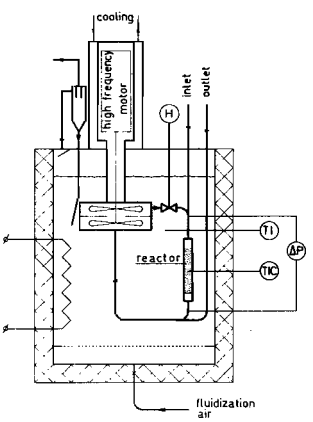

The stainless steel recirculation reactor (figure 2.3) can operate as a plug flow and as a stirred reactor with one quantity of catalyst. The reactor can be switched from the one mode of operation to the other by a valve (H) that is placed in the connection between

the rotating fan and the catalyst holder. Gas purification and analysis is as described for reactor system I. Also the same gases were used. The reactor can operate between 0.1 and 1.0 MPa.

2.5. REACTOR SYSTEM IV: THE PULSE FLOW REACTOR SYSTEM (figure 2.4)

2.5.1. General

A pulse flow reactor is constructed for the transient response experiments. The transient response method can give more definite and first hand information about the kinetics of the elementary steps than steady state experiments do. A number of requirements have to be fulfilled with respect to the construction of this reactor in order to obtain data that can be interpreted easily. These requirements are formulated by Kobayashi and Kobayashi[1]. Firstly, it is preferable to make use of a differential reactor of small diameter to obtain sufficient high superficial gas velocities through the reactor. A second

Figure 2.4. The pulse flow reactor system (IV).

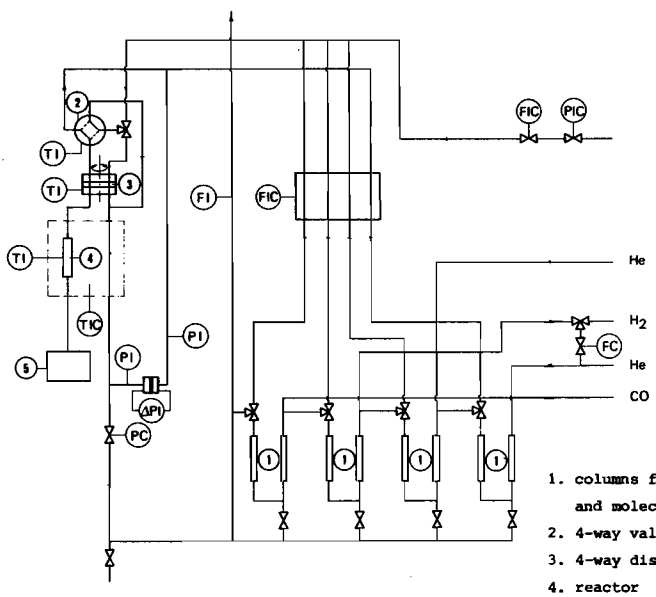

1. columns filled with B.T.S. catalyst and molecular sieve
2. 4-way valve
3. 4-way disc gas sampling valve
4. reactor
5. analysing apparatus

requirement is that the reactor should be equipped with a suitable device that makes it possible to introduce a well shaped step function in the concentration. Finally a suitable analytical device is required that can analyse the reaction components accurately and preferably also continuously.

2.5.2. Apparatus

The stainless steel micro reactor (figure 2.5) is constructed for catalyst pellet sizes of $0.175 \leq d_p$ (mm) ≤ 0.20. The reactor exit is connected via 0.9 m stainless steel capillary (inside diameter 0.2 mm) with the analysing unit. The reactor and part of the capillary is mounted in an electric oven, of which temperature is regulated by a Eurotherm thyristor controller and a chromel-alumel thermocouple.

Figure 2.5. The micro reactor.

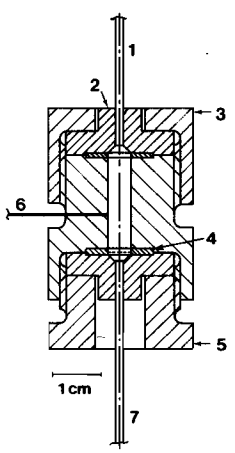

1. reactor inlet
2. collar thrust bearing
3. inlet coupling
4. silver washer
5. outlet coupling
6. thermocouple
7. reactor outlet

A continuous stream of carrier gas passes a four way valve (Whitey) then, the catalyst bed, and flows via a stainless steel capillary into the detector. The carrier gas can be switched to pulse gas with the four way valve. The dead volumes in the four way valve are filled with teflon. The pressure of the pulse gas flow is carefully equalized with that of the carrier gas flow. The pressure in the reactor is determined by the resistance of flow in the capillary. Within

limits the pressure in the reactor can be regulated accurately by adjusting the fraction of the capillary that is in the electric oven. The pressure difference between the carrier gas and the pulse gas is measured with a Hottinger-Baldwin differential pressure detector (PD 1/1). During the experiment, the gas velocities of the carrier and the pulse gas are equal. The gases are regulated by a mass flow controller (P.F.D.-112). The purification of the gases is identical to the procedure followed in reactor system I. In the experiments ultra high purity grade CO is used (Matheson, purity 99.8%) together with helium (Hoekloos, purity 99.995%), hydrogen (Hoekloos, purity 99.9%, and methane (Hoekloos).

2.5.3. Pulse performance

To study the transient behavior of the reacting system, the flow pattern through the apparatus, from the four way inlet valve to the analysing probe should not introduce imported changes in the pulse shape.

Figure 2.6. Response of the pulse flow reactor system to a step in the concentration.

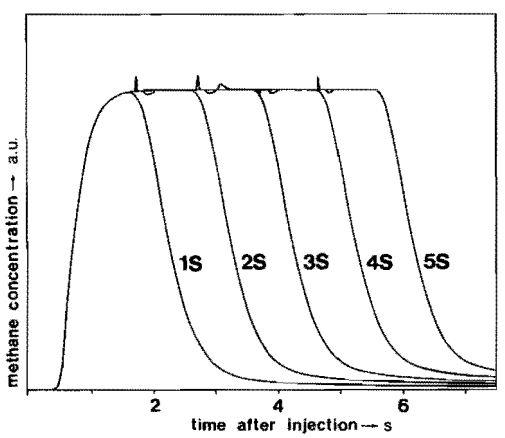

To test how the apparatus behaves in this respect, the response to a concentration step is measured. The concentration step is generated by changing the helium gas stream which flows over the reactor to a mixture of methane and helium. The evolution of methane as a function of time is measured with a Pye-FID-detector, which is connected on line with the reactor exit. During the experiment, the reactor was filled with carborundum ($0.175 \leq d_p \leq 0.20$ (mm)). The reactor was held at a temperature of 520 K, and the total gas flow over the reactor was 0.75 cm^3/s (N.T.P.). The response of the apparatus to the introduction of methane pulses of 1, 2, 3, 4 and 5 seconds duration is shown in figure 2.6. From this graph it can be concluded that the reactor system is suitable for transient experiments if the transient behavior lasts longer than one or two seconds.

REFERENCE

1. Kobayashi, H., Kobayashi, M., Cat. Rev.-Sci. Eng. 10 (2), 139 (1974)

CHAPTER 3

The catalyst

3.1. LITERATURE SURVEY

3.1.1. What we need to know

The present state of the art of catalyst preparation and the understanding of its catalytic behavior bring about that it is generally impossible to design a catalyst for a specific performance on a pure theoretical basis. Catalyst architecture in this sense will ask for a detailed understanding of the reaction mechanism, together with quantitative information about the structure and bonding of the adsorbed reactants, products and reaction intermediates on the surface of the catalyst. Furthermore, information is needed on the effect of catalyst components and other factors, which depend on the conditions and methods of catalyst preparation.

In absence of sufficient data, the important factors determining catalyst behavior can only be speculated on.

3.1.2. Speculations on catalyst behavior

Recently an attempt was made by Büssemeier et al.[1] to predict a suitable catalyst for the production of lower olefines. The authors adopted a theory that relates the synthesis characteristics of the catalyst to its affinity towards synthesis gas components. This relation is also used to explain the promotion effect of alkali (Dry (1969)[2]) and the differences in turnover frequency of various active

metals (Vannice (1975)[3]). This approach is rather popular in the literature of the Fischer-Tropsch synthesis. Its usefulness in predicting catalyst behavior must nevertheless be questioned, because the theories that describe the relation between the adsorption properties of the catalyst and its synthesis characteristics are based on insufficient data. It will be shown that the theories are even contradictory and sometimes inconsistent, and it might be questioned whether a simple relation between catalyst behavior and heat of CO- and H_2-adsorption exists.

Alkali is known to enhance the rate of the hydrocarbon formation and to increase the heat of adsorption of carbon monoxide. Dry et al.[2] correlate the changes in the heat of adsorption and the rate of reaction by adopting the mechanism proposed by Anderson[4], and by defining the formation of the intermediate hydroxyl surface complex as the rate determining step. The molecular orbital treatment of the adsorption of CO by Blyholder[5] shows that an increase in the metal-to-carbon bond strength decreases the strength of the carbon-to-oxygen bond. According to Dry, this weakening of the C-O bond facilitates the attack of hydrogen to form the intermediate hydroxyl surface complex and consequently enhances the rate.

Six years later Vannice[3] uses the same mechanism to explain a correlation between turnover frequency and heat of adsorption of carbon monoxide and hydrogen on different metals. However, not the formation of the hydroxyl surface complex, but its hydrogenation, is claimed to be the rate determining step. The observations are quite contrary to the relation of alkali promotion: an increase of the rate is observed when the heat of CO-adsorption decreases and that of hydrogen increases. According to the argumentation of Vannice it is reasonable to assume that the strength of the metal-to-hydroxyl bond is directly related to the metal-to-carbon monoxide bond strength. Therefore, when the heat of CO-adsorption decreases the concentration of hydroxyl surface species decreases too, and consequently the rate is enhanced by an increased hydrogen surface coverage. The kinetic and adsorption data presented are consistent with the proposed mechanism.

Two years later the flaw became apparent: a correlation between the heat of adsorption of carbon monoxide and the turnover frequency resembles a "volcano plot" (Vannice[6]), a concept based on the ideas of Sabatier[7]. The heat of CO-adsorption on nickel surface is lower

than the optimum value, which means a CO deficiency on the surface during synthesis. In the kinetic model this will result in a low hydroxyl surface coverage and consequently in a positive order in the CO-partial pressure. The kinetic data on nickel however reveal a negative order (-0.31).

3.1.3. Current empirical knowledge

In the absence of fundamental relations to predict catalyst behavior, know-how built up in the past might direct the search for a catalyst that can synthesize light olefines selectivity.

The synthesis of hydrocarbons and other compounds from the catalytic hydrogenation of carbon monoxide has been studied for over 75 years since the work of Sabatier and Senderens (1902)[8]. An enormous amount of information is gathered in the review of Anderson[4] that describes the dynamic period of Fischer-Tropsch catalyst development from 1930 to 1955. Together with the patent literature dealing with olefine selective catalysts, Anderson's work is most likely to contain the useful information. Evaluation of the properties of the catalysts discussed by Anderson leads to the following conclusions:

- The active metal clearly determines the basic catalytic behavior. However, depending on the promotors used, the catalytic characteristics can vary widely;
- Compared to ruthenium, cobalt and nickel, iron shows the most promising intrinsic features to provide a catalyst selective for the production of light olefines;
- A great number of elements are said to show chemical promotion effects for iron catalysts. The elements from Anderson's review, denoted in figure 3.1, are claimed to either decrease the mean molecular weight or increase the olefine content of the synthesis product. The promotors from the patent literature join both characteristics described above.

The transition metals of group IV-VII and the non-metals seem to be the most interesting promoting elements. Although this result is meagre, it is as far as we can get.

In this thesis no results are reported about promotion effects of the transition metals. The element that possesses definite promoting qualities in the required direction, and that will be discussed in this chapter, is the non-metal sulphur.

Figure 3.1. Elements that are claimed to decrease the mean molecular weight, and/or to increase the olefine content of the product from iron catalysts.

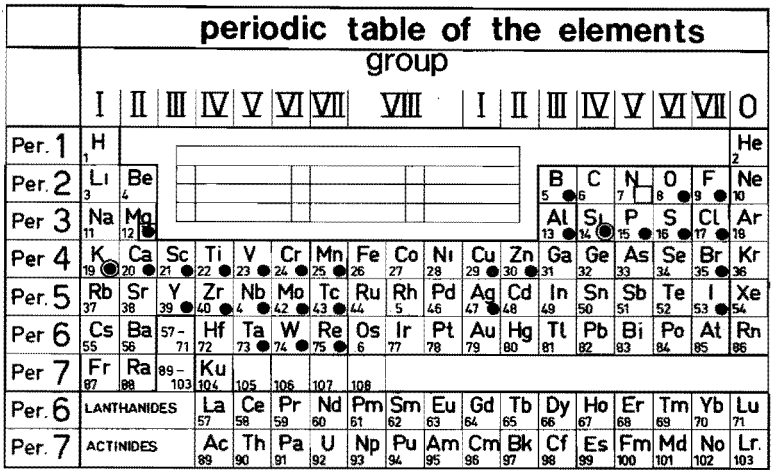

● elements that increase the ethylene and propene content of the product[9-16];

□ elements that decrease the mean molecular weight of the product[4];

○ elements that increase the olefine content of the product[4].

3.1.4. Effect of sulphur

Sulphur is known to be a permanent poison for most of the metal catalysts. In these cases the feed must be thorougly desulphurized to prevent catalyst deactivation. Although the same applies to some extent to the Fischer-Tropsch synthesis (see Anderson[4]), many chemical promotion effects of sulphur are claimed as well. The effect of sulphur described in the literature up to 1977 is reviewed by Madon and Shaw[17]. A decreasing molecular weight and a drop in the degree of saturation of the product by adding up to 4 percent sulphur to the catalyst was already noticed in 1929[9]. Layng[18] and later Davies et al.[12] claim also an increase in the yield of olefinic products upon sulphur addition to iron catalysts. According to Davies,

halogen compounds show characteristics equal to those of sulphur, as is recently confirmed by Hammer et al.[19]. The U.S. Bureau of Mines found that small amounts of sulphur on iron catalysts prevent wax formation and increase the formation of gaseous hydrocarbons[20].

Enikeev and Krylova[21] have offered the hypothesis that sulphur, as an acid promotor, raises the work function of the surface by withdrawing electrons from the metal, thus reducing the capacity of back-bonding of electrons from the metal to the antibonding orbital of carbon monoxide. This implies that the carbon-to-oxygen bond is strengthened, whereas the metal-to-carbon bond is weakened upon sulphur poisoning. This again would result in a decreasing capacity of the catalyst to dissociate carbon monoxide, as has been experimentally confirmed by Kishi and Roberts[22].

3.2. EXPERIMENTAL

3.2.1. The catalyst

Two types of catalysts are discussed in this chapter. Firstly iron catalysts prepared by precipitation of iron-(III)-hydroxide, sometimes

Reference type	Catalyst composition (weight percent)	Raw material	Trade mark	Preparation method
A	$100Fe_2O_3$	$Fe(NO_3)_3 \cdot 9H_2O$	Merck p.a.	precipitation
B	$80Fe_2O_3:20ZnO$	$Fe(NO_3)_3 \cdot 9H_2O$	Merck p.a.	coprecipitation
		$Zn(NO_3)_3 \cdot 4H_2O$	Merck p.a.	
C	$19Fe_2O_3:81Al_2O_3$	$Fe(NO_3)_3 \cdot 9H_2O$	Merck p.a.	impregnation
		γAl_2O_3	Ketjen 006-1.5E	
D	$19Fe_2O_3:81Al_2O_3$	$Fe(NO_3)_3 \cdot 9H_2O$	Merck p.a.	impregnation
		AlOOH	Martinswerk-RH6	
E	$19Fe_2O_3:81SiO_2$	$Fe(NO_3)_3 \cdot 9H_2O$	Merck p.a.	impregnation
		SiO_2	Grace-SP2-324.382	
F	$17Fe_2O_3:9ZnO:74Al_2O_3$	$Fe(NO_3)_3 \cdot 9H_2O$	Merck p.a.	impregnation
		$Zn(NO_3)_2 \cdot 4H_2O$	Merck c.p.	
		γAl_2O_3	Ketjen 006-1.5E	

Table 3.1. Raw catalyst composition.

in combination with zinc-(II)-hydroxide (unsupported catalysts) and secondly iron catalysts prepared by impregnation of alumina- (see appendix 2) and silica-supports with solution, containing iron-(III)- and sometimes zinc-(II)-nitrate (supported catalysts). The composition of the different catalysts are shown in table 3.1.

3.2.1.1. Preparation procedure

3.2.1.1.1. Unsupported catalysts

A double walled vessel is thermostated by circulating water between the inner and outer wall at a temperature of 360 K. The vessel, which has a total volume of 7 dm^3, is filled with 3 dm^3 solution containing 0.5 moles iron-(III)-nitrate and sometimes an additional amount of 0.25 moles zinc-(II)-nitrate. The precipitation is started by the injection of a 0.75 $kmol/m^3$ ammonia solution (Merck p.a.) below the surface of the solution, at a rate of 58 mm^3/s. Central in the vessel a vibrating agitator is mounted to assure homogeneity of the suspension during the precipitation. The precipitation is stopped at a pH value of 8.

The oxidic catalyst is obtained by extensive washing, drying at 395 K for 50 ks and calcining at 675 K for 4 ks. The catalyst can be doped by impregnation with 0.4 cm^3/g cat solution, that contains a specific amount of a chloride or a sulphate salt (Merck p.a.). After this impregnation the drying and calcining procedures are repeated. The surface area calculated from the extent of hydrogen adsorption amounts to 1.7 m^2/g cat.

3.2.1.1.2. Supported catalysts

A solution of 0.12 moles of iron-(III)-nitrate and sometimes an additional amount of 0.06 moles of zinc-(II)-nitrate in 50 cm^3 water at 305 K is used to impregnate 5 g carrier ($0.3 < d_p < 0.5$ (mm)). Prior to the impregnation the carrier is stabilized by heating at 875 K for 9 ks. The saturated carrier is filtered off, and a subsequent drying and calcining procedure, identical to that of the precipitated catalyst, yields the raw batch. Iron sulphate is administered to these catalysts in a doping step.

3.2.2. *Continuous flow experiments*

3.2.2.1. *Standard catalyst*

The activity and selectivity of the catalysts are studied in a continuous flow fixed bed reactor system (I) described in chapter 2. The catalysts are subjected to standard tests, of which the operation conditions are denoted in table 3.2, block 1.

Block	Catalyst	Total pressure (kPa)	Space time (NTP) ((W/F) g cat.s/m^3) H_2 reduction	Space time (NTP) ((W/F) g cat.s/m^3) Synthesis	L/dp	D/dp	Feed composition x_{H_2} reduction	Feed composition Synthesis $x_{H_2}:x_{CO}:x_{IIc}$	H_2 reduction time (ks)	Temperature (K) H_2 reduction	Temperature (K) Synthesis
	STANDARD CATALYST TEST										
1	prepared by precipitation	100	3.6×10^5	3.6×10^5	42	15	1.0	0.2;0.2;0.6	58	625	525 or 625
	prepared by impregnation	100	7.2×10^5	7.2×10^5	125	15	1.0	0.2;0.2;0.6	58	625	625
	CATALYST TEST with H_2S adsorption										
2	$80Fe_2O_3:20ZnO$ (B)	100	H_2S ADSORPTION 1.2×10^5		111	10				525	
		100	REDUCTION & SYNTHESIS 3.6×10^5	3.6×10^5	111	10	1.0	0.2;0.2;0.6	58	625	625
	LONG PERIOD TEST										
3	$19Fe_2O_3:81Al_2O_3$ (C) + 1×10^{-3} g/g cat $Fe_2(SO_4)_3$	100	4.8×10^6	$0.8\text{-}4.8\times10^6$ variable	125	12	1.0	0.2-0.8; 0.2-0.8; 0.0-0.6 variable	50	625	625
	$80Fe_2O_3:20ZnO$ (B) + 16×10^{-3} g/g cat $Fe_2(SO_4)_3$	100	1.4×10^5	$0.2\text{-}4.8\times10^6$ variable	170	15	1.0	0.2-0.8; 0.2-0.8; 0.0-0.6 variable	58	625	625
	$80Fe_2O_3:20ZnO$ (B) + 35×10^{-3} g/g cat $Fe_2(SO_4)_3$	100 - 600 variable	3.6×10^6	$0.6\text{-}3.6\times10^6$ variable	16	13	1.0	0.2-0.8; 0.2-0.8; 0.0-0.6 variable	58	625	525 - 625 variable

Table 3.2. Operation conditions of the catalyst tests.

3.2.2.2. *H_2S-doped catalysts*

In the combined pulse- and continuous-flow fixed bed reactor system (II), described in chapter 2, hydrogen sulphide is pulsed in quantities of 8.5×10^{-6} mol/pulse on the reduced catalyst at high space velocity to prevent preferential adsorption at the inlet portion of the bed. The non-adsorbed hydrogen sulfide, emerging from the outlet of the reactor, is fixed by a solution of zinc acetate. The quantity of H_2S adsorbed on the catalyst is calculated from the difference of the amount of H_2S pulsed and the amount of H_2S determined by quantitative analysis on the zinc acetate solution by jodometric titration[23]. After the H_2S-adsorption, the performance of the catalysts in the synthesis reaction is tested at 625 K. The process conditions of reduction, adsorption and synthesis are shown in table 3.2, block 2.

3.2.2.3. *Catalyst stability*

The process conditions used in the experiments to test the stability of the catalyst are shown in table 3.2, block 3. Catalysts 19 Fe_2O_3 : 81 Al_2O_3(C) + 1 x 10^{-3} g $Fe_2(SO_4)_3$/g cat and 80 Fe_2O_3 : 20 ZnO(B) + 3.5 x 10^{-2} g $Fe_2(SO_4)_3$/g cat are tested in the continuous stirred gas-solid reactor system (III), described in chapter 2. The latter catalyst is packed between particles of alumina. The experiment with catalyst 80 Fe_2O_3 : 20 ZnO(B) + 1.6 x 10^{-2} g $Fe_2(SO_4)_3$/ g cat is performed in the reactor system I, described in chapter 2.

3.2.3. *Thermogravimetric analysis*

Changes in weight, mainly due to carbon deposition on the catalyst by interaction with synthesis gas is studied in a Dupont 950 thermogravimetric analyser. The experiments are carried out at 100 kPa. The method of gasregulation and gas-clean-up is the same as described for the continuous flow fixed bed reactor (I) (chapter 2). A combination of a chromel-alumel thermocouple in the electrical furnace and a Eurotherm thyristor controller, equipped with a motor attached to the thumbwheel, permits isothermal and temperature-programmed operation of the balance. The actual temperature is measured within the sample

chamber just above the quartz sample holder. The control end of the balance is continuously purged with helium (0.16 cm^3/s) to avoid contamination.

3.2.4. Carbon analysis

For a number of catalysts, the amount of carbon formed during the standard continuous flow experiment is determined with a F&M carbon-hydrogen-nitrogen-analyser. To prevent oxidation of the carbon deposits, the reactor with the catalyst sample is opened to air after a helium flush of 3.5 ks, and the catalyst is removed from the reactor after 86 ks. By this procedure pyrophoric phenomena are avoided.

3.2.5. Adsorption experiments

For the adsorption experiments a Pyrex glass apparatus is used. After in situ reduction in hydrogen of the catalyst sample (about 2 g), the system is evacuated at 625 K for 3.5 ks. Hydrogen adsorption is measured by admitting 1.8 kPa of pure hydrogen at 625 K and subsequent cooling to room temperature. Carbon monoxide is measured by cooling the reduced and evacuated catalyst to room temperature, and thereafter admitting 2.0 kPa carbon monoxide (first adsorption). After the first adsorption the catalyst is evacuated for 3.5 ks at room temperature, whereafter a second adsorption identical to the first is performed. The difference between the first and the second adsorption is defined as the amount of chemisorbed CO. Two Leybold-Heraeus pumps can provide a minimum pressure of 0.1 kPa.

3.3. RESULTS AND DISCUSSION

It is frequently suggested in the literature[24-26] that activity and selectivity of iron catalysts are determined by carbon depositions on the catalyst surface and phase transformations in the bulk of the catalyst. Therefore, the synthesis performance of the catalyst is described together with the carbon analysis of the catalyst after synthesis, and thermogravimetric analysis of the carbon deposition during the synthesis.

3.3.1. Activity and selectivity

3.3.1.1. Unsupported catalysts

3.3.1.1.1. Influence of temperature and iron-sulphate promotion

In this paragraph two factors that largely determine the activity and selectivity of the iron catalyst viz. temperature and iron sulphate content, will be discussed. The olefine selectivity will alternatively be defined in this chapter as the rate of formation of olefines with n carbon atoms devided by the rate of formation of hydrocarbons with n carbon atoms (see appendix 1).

Figure 3.2. The rate of carbon monoxide conversion to hydrocarbons ($r_{T,4}$) of iron/zinc oxide catalysts as a function of time. $x_{CO} = x_{H_2} = 0.2$.
Curve a: sulphate free catalyst at 525 K.
Curve b: sulphate free catalyst.
Curve c: catalyst with 8.0 mg $Fe_2(SO_4)_3$/g cat.
Curve d: catalyst with 33 mg $Fe_2(SO_4)_3$/g cat.
The reaction temperature in experiments b, c and d is 625 K.

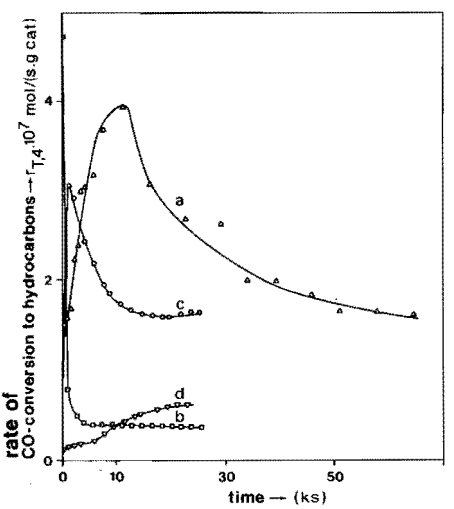

Curve a of figure 3.2 shows that at 525 K the iron-zinc-oxide catalyst (cat. B) is gradually activated in the synthesis gas mixture, and that, after reaching an activity maximum, the catalyst slowly

deactivates. Curve b represents the activity changes of the same catalyst at 625 K. Clearly, much less time is involved in the activation and deactivation of the catalyst, and the steady state activity level is very low. When the catalyst is impregnated with iron sulphate (curves c, d), the activation and deactivation at 625 K is again retarded. The steady state activity seems to depend on the amount of iron sulphate added to the catalyst. Table 3.3 represents the selectivities as defined in appendix 1 after 22 ks of operation, when a nearly constant hydrocarbon production has been obtained.

$Fe_2(SO_4)_3$ content (g/g catalyst)	Operation temperature (K)	Methane selectivity ($SC_{1,4}$)	Ethylene selectivity (OC_2)	Propylene selectivity (OC_3)
none	523	.37	.53	.86
none	623	.70	.92	1.00
8.0×10^{-3}	623	.28	.97	.99
$3\ 3 \times 10^{-3}$	623	.23	.99	1.00

Table 3.3. Product selectivities of iron-zinc oxide catalysts when a steady state hydrocarbon production is obtained, $x_{CO} = x_{H_2} = 0.2$.

While both the methane selectivity and the olefine selectivity increase as the temperature is raised, only the methane selectivity is suppressed by adding iron sulphate to the catalyst. The decrease of the methane selectivity upon impregnation of the catalyst with iron sulphate, can be a consequence of either an increased ratio of the rate of propagation versus the rate of termination for the C_2-C_5 fraction or of a decrease of the rate of methane production. A Schulz-Flory type plot shows that the latter alternative is realized (compare curves b and c of figure 3.3).

The increased olefine selectivity of the undoped catalyst, obtained when the temperature is raised from 525 to 625 K, gives no increase in the quality of the reaction product due to the high methane production. The ratio of the rate of CO-conversion to ethene plus propene and the rate of CO-conversion to hydrocarbons, changes from 0.29 at

Figure 3.3. A Schulz-Flory type plot of the hydrocarbon product of a iron/zinc oxide catalyst at steady state. $x_{CO} = x_{H_2} = 0.2$. *△ sulphate free catalyst at 525 K; □ sulphate free catalyst at 625 K; ○ catalyst with 8.0 mg* $Fe_2(SO_4)_3$*/g cat at 625 K.*

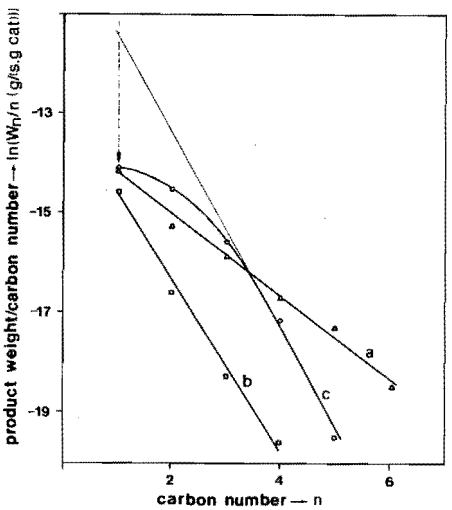

Catalyst		80 Fe_2O_3 : 20 ZnO (B)	80 Fe_2O_3 : 20 ZnO (B)
$Fe_2(SO_4)_3$ content (g/g cat)		none	8×10^{-3}
Temperature (K)		525	625
CH_4	(%)	37	28
C_2H_6	(%)	11	1
C_2H_4	(%)	12	42
C_3H_8	(%)	3	0
C_3H_6	(%)	17	22
$C_{4,T}$	(%)	13	6
$C_{5,T}$	(%)	7	1
$P_{T,5}$	(%)	100	100
$(C_2H_5 + C_3H_6)$	(%)	29	64

Table 3.4. Contribution of the different hydrocarbons to the conversion of carbon monoxide to hydrocarbons $(r_{T,5})$, $x_{CO} = x_{H_2} = 0.2$.

525 K to 0.25 at 625 K. To show that selectivities in the product distribution of the undoped catalyst do have changed as a function of temperature, the alternative definition of the olefine selectivity is used in this chapter (see table 3.3).

The attractiveness of a combination of temperature increase and sulphate-addition for the production of lower olefines is illustrated in table 3.4.

Figure 3.4. Characteristics of iron/zinc oxide catalysts as a function of iron sulphate content (data of the steady state synthesis at 625 K; $x_{CO} = x_{H_2} = 0.2$).
▽ CO-conversion to hydrocarbons ($r_{T,4}$)
○ ethene selectivity (OC_2)
△ methane selectivity ($SC_{1,4}$)

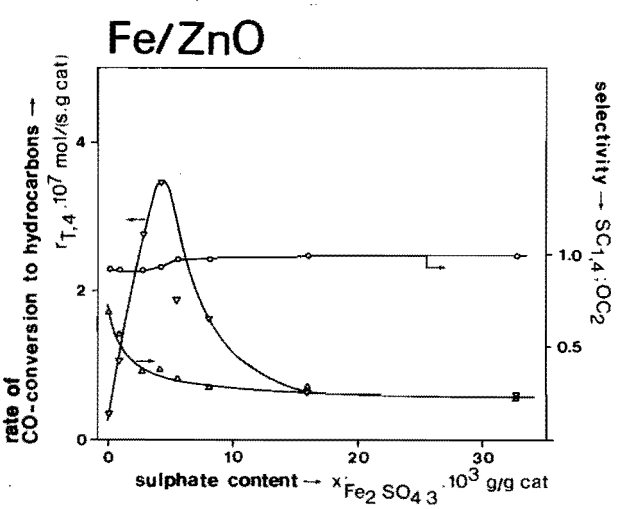

The activity and selectivity data obtained at the end of a standard continuous flow experiment at 625 K (after about 25 ks) as a function of the iron sulphate content of the catalyst, are assembled in figures 3.4 and 3.5. By increasing the iron sulphate concentration of the unsupported iron catalysts, the steady state synthesis activity reaches a maximum at 4.0 mg $Fe_2(SO_4)_3$/g.cat, the methane selectivity drops monotonuously and the olefine selectivity is only minimally affected. Zinc oxide retards the poisoning effect of iron sulphate at high concentrations.

Figure 3.5. Characteristics of pure iron catalysts as a function of iron sulphate content (data of the steady state synthesis at 625 K; $x_{CO} = x_{H_2} = 0.2$).
▽ CO-conversion to hydrocarbons ($r_{T,4}$).
○ ethene selectivity (OC_2).
△ methane selectivity ($SC_{1,4}$).

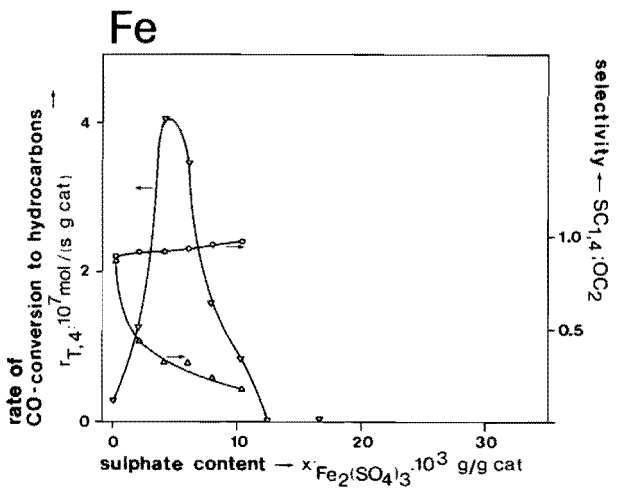

3.3.1.1.2. Further tests of the sulphate promotion

To test the specificity of the sulphate-ion in determining the selectivity of precipitated iron catalysts at high temperature synthesis, an iron-zinc oxide catalyst (B) is impregnated with different sulphate salts and with iron chloride. Furthermore the effect of hydrogen sulphide additions to this catalyst is investigated. The activity and methane selectivity in the steady state of the catalyst upon addition of different salts, can be compared in table 3.5. The results show that sulphate salts all have about the same influence. Addition of iron chloride only deactivates the catalyst: during the whole standard test the activity never exceeds a hydrocarbon production of $r_{T,5}$ = 0.08 mmol/s.kg cat, and no decrease of the methane selectivity is observed as compared to the undoped catalyst. The activity and selectivity data obtained from the experiments described

Catalyst	Type of salt added	Impregnated amount on anion basis (moles/g cat)	CO conversion to hydrocarbons ($r_{T,5}$) (moles/(s.g cat))	Methane selectivity ($SC_{1,5}$)
80 Fe_2O_3 : 20 ZnO (B)	$Fe_2(SO_4)_3$	6.0×10^{-5}	1.5×10^{-7}	.28
	$(NH_4)_2\ SO_4$	6.0×10^{-5}	2.2×10^{-7}	.36
	Zn SO_4	6.0×10^{-5}	1.8×10^{-7}	.31
	$Na_2\ SO_4$	6.0×10^{-5}	8.9×10^{-8}	.26
	Fe Cl_3	6.0×10^{-5}	1.7×10^{-8}	.90
	none	none	3.5×10^{-8}	.70

Table 3.5. The influence of various salts on the steady state activity and selectivity of iron-zinc oxide unsupported catalysts at 625 K, $x_{CO} = x_{H_2} = 0.2$.

in paragraph 3.2.2.2 for catalysts to which different amounts of H_2S have been admitted are shown in table 3.6. Here no promotion effects comparable to those reported for sulphate are noticed.

Catalyst	H_2S charge (moles/g cat)	Equivalent $Fe_2(SO_4)_3$ charge on sulphur basis ($gFe_2(SO_4)_3$/g cat)	CO conversion to hydrocarbons ($r_{T,3}$) (moles/(g cat.s))	Methane selectivity ($SC_{1,3}$)
$80Fe_2O_3$:20ZnO (B)	none	none	3.5×10^{-8}	.72
	4.1×10^{-5}	5.5×10^{-3}	1.6×10^{-8}	.75
	8.8×10^{-5}	1.2×10^{-2}	1.1×10^{-8}	.77
	1.7×10^{-4}	2.3×10^{-2}	7.8×10^{-9}	.75

Table 3.6. The influence of H_2S on the steady state activity and selectivity of unsupported iron-zinc oxide catalysts at 625 K, $x_{CO} = x_{H_2} = 0.2$.

3.3.1.2. Supported catalysts

In this paragraph the results are discussed of synthesis experiments performed to test whether sulphate promotion is also applicable to supported iron catalysts. The catalysts are submitted to standard continuous flow experiments, as described in the experimental section.

Reference	Catalyst	$Fe_2(SO_4)_3$ impregnated x 10^{-3} (g/g cat)	CO conversion to hydrocarbons x 10^{-8} (mole/(s.g cat)) ($r_{T,5}$)	Type of support	Methane selectivity $SC_{1,5}$	Ethylene selectivity OC_2	Propylene selectivity OC_3
C	$19Fe_2O_3:81Al_2O_3$	none	11.7	Ketjen	.25	.91	.96
F	$17Fe_2O_3:9ZnO:74Al_2O_3$	none	12.5	Ketjen	.30	.91	.94
C	$19Fe_2O_3:81Al_2O_3$	.96	9.5	Ketjen	.24	.92	.97
C	$19Fe_2O_3:81Al_2O_3$	4.80	5.6	Ketjen	.20	.92	.97
F	$17Fe_2O_3:9ZnO:74Al_2O_3$	.86	7.7	Ketjen	.23	.91	.95
F	$17Fe_2O_3:9ZnO:74Al_2O_3$	4.30	1.7	Ketjen	.22	.93	.98
D	$19Fe_2O_3:81Al_2O_3$	none	.6	Martinswerk	.48	1.0	1.0
E	$19Fe_2O_3:81SiO_2$	none	2.3	Grace	.49	.95	.95

Table 3.7. Steady state synthesis characteristics of supported iron catalysts at 625 K, $x_{CO} = x_{H_2} = 0.2$.

Surprisingly, it turned out to be possible to prepare a catalyst by impregnation of an alumina carrier without any sulphate addition, exhibiting the same steady state production characteristics as the sulphated precipitation catalysts (compare table 3.7, block 1 and figure 3.6 with table 3.3 and figure 3.3). No large selectivity improvements are obtained upon sulphate addition, but a severe reduction in activity of the catalyst occurs (table 3.7, block 2). Although it is not possible to prove irrefutably that sulphate also has a role in the product selectivity of the supported catalysts to which no sulphate has been purposely added, evidence strongly points in this direction, as the specification of the gamma-alumina used, shows that it contains an appreciable amount of sulphate salts (see appendix

Figure 3.6. A Schulz-Flory type plot of the hydrocarbon product of supported iron catalysts at steady state. $x_{CO} = x_{H_2} = 0.2$, *T = 625 K.*

▽ *catalyst 17* Fe_2O_3 *: 9 ZnO : 74* Al_2O_3*; no sulphate added (Ketjen support).*

△ *catalyst 19* Fe_2O_3 *: 81* Al_2O_3*; no sulphate added (Ketjen support).*

□ *catalyst 19* Fe_2O_3 *: 81* Al_2O_3*; no sulphate added (Martinswerk support).*

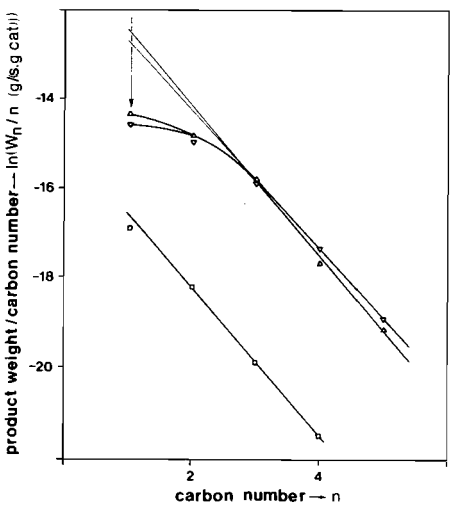

When this carrier is slurried in diluted nitric acid, the presence of sulphate ions can be demonstrated in the liquor. This proves that these sulphate salts will be dissolved to some extent during the impregnation procedure and, thus, that they will precipitate on the iron during drying of the catalyst.

To approach the problem from an other angle, two impregnation catalysts were prepared with chemically pure carriers. The results of the continuous flow experiments with these catalysts, depicted in figures 3.6 and 3.7 and table 3.7 (block 3), show more similarity with the sulphate-free precipitation catalysts, then the catalysts based on the technical grade alumina.

Figure 3.7. The rate of carbon monoxide conversion to hydrocarbons of supported iron catalysts as a function of time. $x_{CO} = x_{H_2} = 0.2$. *T = 625 K.*

▽ *catalyst 17* Fe_2O_3 : *9 ZnO : 74* Al_2O_3 *(Ketjen support).*

△ *catalyst 19* Fe_2O_3 : *81* Al_2O_3 *(Ketjen support).*

□ *catalyst 19* Fe_2O_3 : *81* Al_2O_3 *(Martinswerk support).*

○ *catalyst 19* Fe_2O_3 : *81* SiO_2 *(Grace support).*

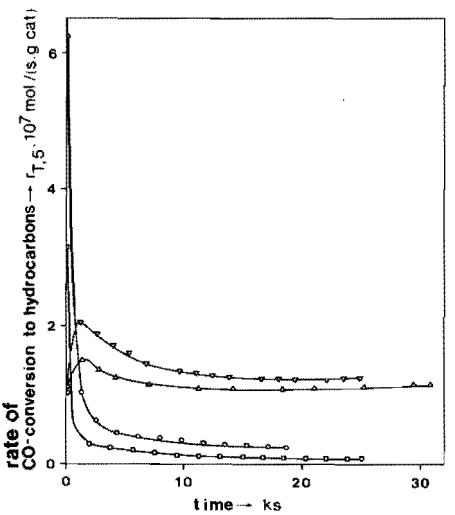

3.3.1.3. Conclusions

The conclusions obtained so far can be summarized by the following statements:

1. The combination of high temperature synthesis and sulphate salt addition raises the olefine content of the product, and selectively suppresses the methane formation of unsupported iron catalysts and decreasing the formation of hydrocarbons higher than C_3;
2. There is an optimum in the steady state activity of the unsupported catalysts at 625 K as a function of the sulphate content;
3. Addition of zinc oxide causes the activity to remain at a reasonable level at the higher sulphate concentrations;
4. The chemical promotion effects are only obtained by addition of sulphate salt; no positive promotion effect has been found for

application of iron chloride or hydrogen sulphide;

5. It is likely that the effect of sulphate on the synthesis performance of supported catalysts is simular to the promotion reported for unsupported catalysts.

A surprising discrepancy between this work and the literature on the effect of sulphur, is that we found it impossible to obtain the same promotion from sulphide as from sulphate. According to the first patent that claims sulphur promoting effects on iron catalysts[9], alkali sulphide, alkali hydrosulphide or hydrogen sulphide can be used; also Davies et al.[12] and Layng[18] use volatile sulphur compounds. The discrepancy is even more remarkable, because qualitative sulphide analysis shows that the sulphate-doped-unsupported-catalyst after the synthesis experiment contains sulphide, while in the raw sulphate-impregnated sample no sulphide can be detected. This means that during reduction and/or synthesis the sulphate ion is reduced to the sulphide. Evidently, the way of introducing sulphur to the catalyst is of crucial importance. Pore diffusion can offer an explanation why there is no similarity between the synthesis characteristics of our hydrogen sulphide- and iron sulphate-treated catalysts. The behavior of H_2S-poisoned catalysts (see table 3.6) in the synthesis can be understood when the treatment of the iron catalyst with hydrogen sulphide is performed in a diffusion controlled regime. In that case the poisoning of the catalyst occurs because all the hydrogen sulphide that is admitted is adsorbed on the outside, causing high surface concentrations of sulphide. When during such shell deactivation the quantity of H_2S admitted is increased, the front of the deactivated region moves inwards. According to this model two phases are present in the catalyst pellet: a completely deactive zone and in inner active unpromoted zone. In contrast, sulphate impregnation changes the characteristics of the catalyst pellet uniformly.

The ability of sulphur, as an acid promotor, to decrease the bond strength of carbon monoxide to the iron surface, as postulated by Enikeev and Krylova[21] and experimentaly proved by Kishi and Roberts[22], is confirmed by adsorption measurements. Carbon monoxide and hydrogen adsorption experiments are performed according to the procedure described in paragraph 3.2.5. The results of the adsorption and the standard synthesis tests are shown in table 3.8. Although the hydrogen adsorption stays constant or even shows a slight increase, the carbon

	SYNTHESIS		ADSORPTION	
Catalyst 80 Fe_2O_3 : 20 ZnO	Synthesis activity at 625 K $x_{CO} = x_{H_2} = 0.2$ $(r_{T,3})$ (mol/(s.g cat))	Methane selectivity $SC_{1,3}$	H_2-adsorption (mol/g cat)	CO-adsorption (mol/g cat)
no sulphate added	2.0×10^{-8}	.72	1.3×10^{-5}	2.1×10^{-5}
$(NH_4)_2 SO_4$ added	2.3×10^{-8}	.33	1.6×10^{-5}	1.4×10^{-6}

Table 3.8. Adsorption and synthesis properties of unsupported iron-zinc oxide catalysts.

monoxide adsorption decreases by a factor of 15, which clearly demonstrates the decreased affinity of the catalyst towards carbon monoxide. This agrees with the tenfold reduction reported by Wentrcek et al.[27] in the CO-adsorption on a Ni/Al_2O_3 catalyst upon H_2S-poisoning.

3.3.2. Carbon deposition

Carbon deposition on the iron catalyst comprises both the formation of iron carbide structures and the deposition of elemental carbon (free carbon).

3.3.2.1. Unsupported catalysts

The carbon content of the catalyst after the continuous flow experiments is shown in figure 3.8. The actual rate of carbon deposition can be calculated at any moment from the massbalance:

$$\text{rate of carbon deposition} = r_T - (rCO_2 + rH_2O)$$

The values for the rate of carbon deposition at the end of the standard synthesis experiment, as shown in figure 3.8 together with the carbon content of the catalyst, are only indicative values, because

Figure 3.8. The rate of carbon deposition at 625 K after approximately 22 ks synthesis (o), and the accumulated amount of carbon deposited on the catalyst over this period (□), as a function of sulphate content of the catalyst. $x_{CO} = x_{H_2} = 0.2$. *Figure a: the results of a 80* Fe_2O_3 *: 20 ZnO catalyst. Figure b: the results of a 100* Fe_2O_3 *catalyst.*

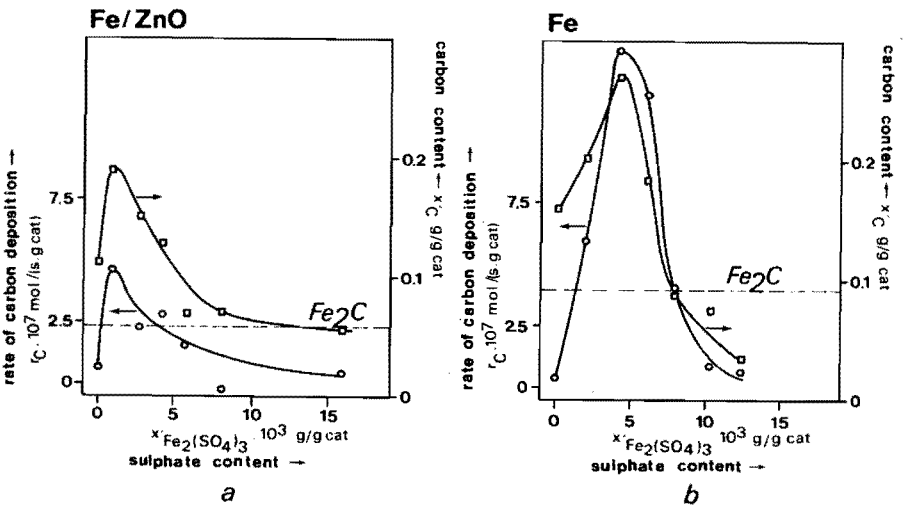

of the inaccurate water analysis. Because Fe_2C is the carbon richest carbide known, the Fe_2C-lines in this figure show the maximum carbide content of the catalyst. If the contribution of adsorbed reactants and hydrocarbons to the carbon content is neglected, catalysts that have a carbon content higher than the Fe_2C must contain free carbon.

The results indicate that small iron sulphate additions enhance the rate of free carbon deposition over a period of time longer than the time needed to get a constant hydrocarbon production. Rather large quantities of iron sulphate have to be used to keep the carbon content of the catalysts below the Fe_2C-carbide level. No explicit relation between steady state hydrocarbon productivity and carbon content of the catalyst can be deduced from the results described above.

When in the isothermal gravimetric analysis a sulphate free iron zinc oxide catalyst is exposed to synthesis gas at 625 K (figure 3.9

Figure 3.9. Isothermal gravimetric analysis of the carbon deposition on iron/zinc oxide catalysts at 625 K (catalyst 80 Fe_2O_3 : 20 ZnO), $x_{CO} = x_{H_2} = 0.2$.
Curve a: sulphate free catalyst.
Curve b: catalyst containing 4.2 mg $Fe_2(SO_4)_3$/g cat.
Curve c: catalyst containing 16 mg $Fe_2(SO_4)_3$/g cat.
Curve d: catalyst containing 35 mg $Fe_2(SO_4)_3$/g cat.
Conditions:
◇ *$0.4 \leqq d_p \leqq 0.6$ (mm); F = 2.8 (cm^3/s);*
● *$0.09 \leqq d_p \leqq 0.15$ (mm); F = 2.8 (cm^3/s);*
□ *$0.15 \leqq d_p \leqq 0.21$ (mm); F = 1.4 (cm^3/s);*
○ △ ▽ *$0.15 \leqq d_p \leqq 0.21$ (mm); F = 2.8 (cm^3/s).*

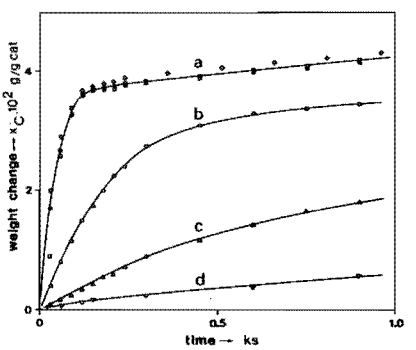

curve a) two distinct stages in the carbon deposition can be distinguished. The first stage can be ascribed to a fast conversion of iron to Fe_2C, and the second stage to the much slower deposition of free carbon. When iron sulphate is added to the catalyst the rate of carbidisation is retarded (figure 3.9, curves b, c, d). Figure 3.10 shows that the carbon deposition of free carbon on the catalyst (presented by curve b, figure 3.10) accelerates after the Fe_2C formation has been completed. The deposition of free carbon need not change the activity of the catalyst to produce hydrocarbons, as is illustrated in figure 3.11.

Figure 3.10. Isothermal gravimetric analysis of the carbon deposition on iron/zinc oxide catalysts at 625 K (catalyst 80 Fe_2O_3 : 20 ZnO) $x_{CO} = x_{H_2} = 0.2$.
Curve a: sulphate free catalyst.
Curve b: catalyst containing 4.2 mg $Fe_2(SO_4)_3$/g cat.
Curve c: catalyst containing 16 mg $Fe_2(SO_4)_3$/g cat.
Curve d: catalyst containing 35 mg $Fe_2(SO_4)_3$/g cat.
Conditions:
$0.15 \leq d_p \leq 0.21$ (mm); F = 2.8 (cm^3/s).

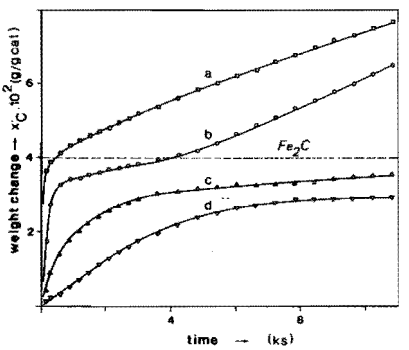

Figure 3.11. Synthesis performance of, and carbon deposition on a 80 Fe_2O_3 : 20 ZnO catalyst containing 4.2 mg $Fe_2(SO_4)_3$/g cat, as a function of time.
o Carbon deposition (isothermal gravimetric analysis).
Δ CO-conversion to hydrocarbons (synthesis experiment).

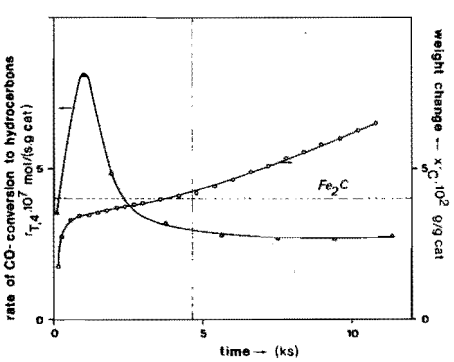

Another method to determine the activity of the catalyst for carbide and free carbon formation, is by temperature programmed thermogravimetric analysis (TPGA). The curves shown in figure 3.12 represent the weight changes due to carbon deposition on exposure to synthesis gas at a heating rate of 0.083 K/s. The impregnation with iron sulphate retards the formation of ironcarbide, but only at the highest sulphate concentration a strong retardation of the free carbon deposition is noticed.

Figure 3.12. Temperature programmed gravimetric analysis of the carbon deposition on iron/zinc oxide catalysts at 625 K.
$x_{CO} = x_{H_2} = 0.2$.
□ *Sulphate free catalyst.*
○ *Catalyst containing 4.2 mg* $Fe_2(SO_4)_3$*/g cat.*
△ *Catalyst containing 16 mg* $Fe_2(SO_4)_3$*/g cat.*
▽ *Catalyst containing 35 mg* $Fe_2(SO_4)_3$*/g cat.*
Conditions:
$0.15 \leqq d_p \leqq 0.21$ *(mm); F = 2.8* (cm^3/s).

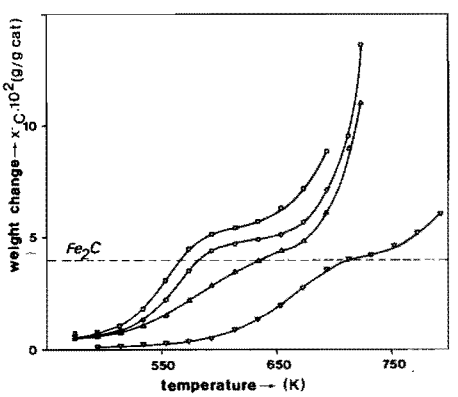

3.3.2.2. *Supported catalysts*

The TPGA of the carbon deposition on supported catalysts at a heating rate of 0.083 K/s, as represented in figure 3.13, shows that the formation of free carbon on impregnation catalysts with chemical

pure carriers starts at about 620 K, while on a catalyst containing sulphate the free carbon deposition is delayed to a temperature of approximately 680 K.

Figure 3.13. Temperature programmed gravimetric analysis of carbon deposition on supported iron catalysts at 625 K.
$x_{CO} = x_{H_2} = 0.2$.
● *19* Fe_2O_3 *: 81* SiO_2 *(E); no sulphate added.*
■ *19* Fe_2O_3 *: 81* Al_2O_3 *(D); no sulphate added.*
◇ *19* Fe_2O_3 *: 81* Al_2O_3 *(C); 0.96 mg* $Fe_2(CH_4)_3$*/g cat added.*
Conditions:
$0.15 \leq d_p \leq 0.21$ *(mm); F = 2.8* (cm^3/s).

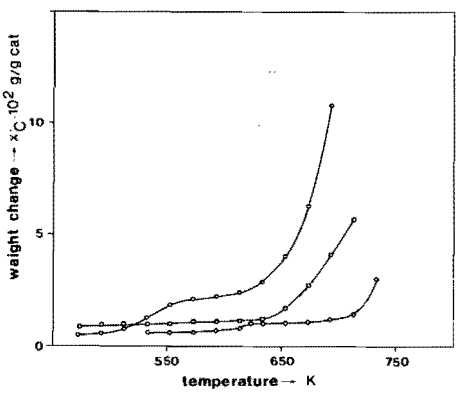

3.3.2.3. Conclusions

In figure 3.14 the results of the carbon deposition on the prepared catalysts are summarized. This figure shows that the doping of iron catalysts with sulphate salts slows down the carbidization of the catalyst. However, the catalyst with a low sulphate content shows an increased activity towards carbon deposition during the synthesis. With respect to this latter phenomenon, we notice that the sulphate doping effect is the reverse of the reported effect of alkali, e.g. low alkali concentrations in the catalyst tend to retard carbon deposition, while the carbon formation is enhanced when higher charges are used (> 0.2 weight percent K_2CO_3[28-30]).

Figure 3.14. Summary of the effect of sulphate on the carbon deposition on iron catalyst during the synthesis. $x_{CO} = x_{H_2} = 0.2$, $T = 625$ *K.*

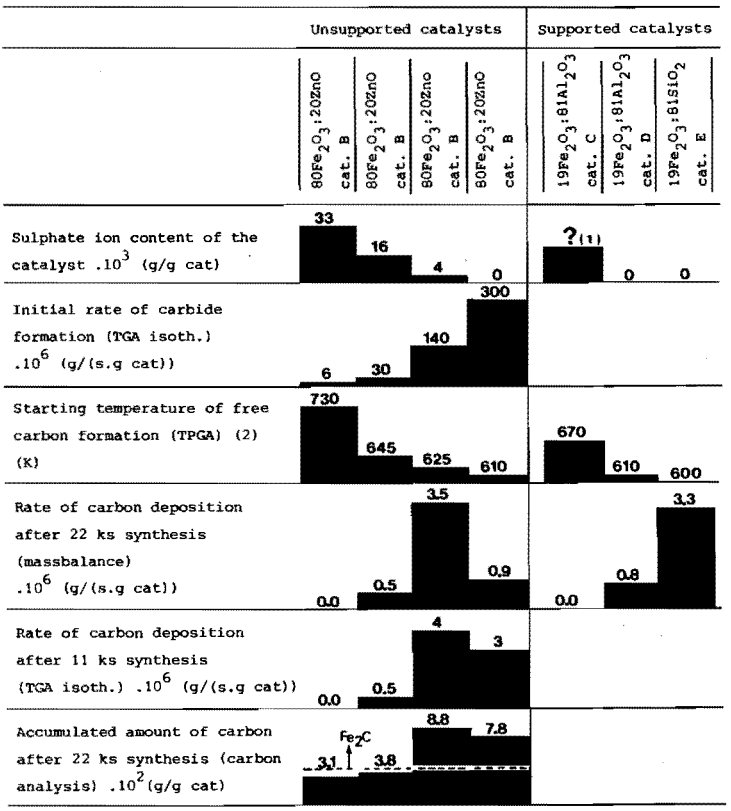

(1) The total sulphate content of the $19Fe_2O_3:81Al_2O_3$ (C) catalyst is not known, due to an unknown amount of carrier sulphate. An additional amount of 0.96 mg $Fe_2(SO_4)_3$/g cat is impregnated.

(2) For the starting temperatures of free carbon deposition, the temperatures at the points of inflection are taken between the carbide and the free carbon formation.

Three different stages can be distinguished in the carbon deposition as shown in figure 3.11. Initially, when the catalyst is carburized, the synthesis activity increases. As the total carbon content of the catalyst reaches a value that corresponds to $Fe_{2.2}C$, the rate of carbon deposition decreases, and so does the synthesis activity of the catalyst. This period of relative slow carbon deposition

and deactivation is followed by a third stage, in which further carbon deposition causes no change in the synthesis activity. Dwyer and Somerjai[26] state that the deactivation of iron catalysts can be explained by the deposition of a carbon overlayer on the active carbided surface. From our results we conclude that there are two types of free carbon deposits:

1. a carbon layer that encapsulates a part of the active surface, and thus reduces the synthesis activity;
2. carbon deposits that have no influence on the synthesis activity.

With respect to the latter type of carbon, it is possible, that they are formed by decomposition of the iron carbide. The iron carbides formed under synthesis conditions are thermodynamically unstable with respect to their elements (in their stablest form).

The maximum amount of surface covered by the first type of carbon at steady state operation is reached when the deactivation rate is equal to the regeneration rate. The deactivation reaction is the surface encapsulation and the regeneration reaction is the hydrogenation of encapsulating carbon. The steady state coverage where equal rate is obtained between encapsulation and hydrogenation will depend on the process conditions and the type of catalyst. It is shown by adsorption and carburization experiments that sulphate doping reduces the affinity of the catalyst to carbon containing compounds, and that the catalyst capacity for hydrogen is not influenced. Furthermore, we have found that the reaction order in carbon monoxide is positive on sulphate containing catalysts, while on pure iron orders equal or less than zero are measured[3,31,32]. These results show that the surface coverage of the sulphate containing catalyst with monocarbon species is lower than on the undoped catalyst. This means that the rate of encapsulation, which will be a function of the amount of monocarbon species, is reduced by sulphate addition, while the rate of hydrogenation of encapsulated carbon is not changed correspondingly. Therefore it is understandable that the steady state hydrocarbon production is increased when small amounts of sulphate are added to the catalyst. When higher concentrations of sulphate are used, the poisoning effect of sulphate will overcome the reduced encapsulation activity.

Hence, the major processes for carbon deposition are: the formation of carbon species on the surface, the dissolution of carbon species

in the bulk with formation of iron carbides, and the build-up of a carbon agglomerate on the active surface. The iron carbides formed can in their turn decompose into carbon and iron. This qualitative model is in agreement with that proposed by Cooper and Trimm[33] for the carbon deposition from propene on iron, and that of the growth of carbon deposits from acetylene on nickel and iron as published by Baker et al.[34].

In principle, the total carbon content of the catalyst can be composed of carbides, free carbon, carbon oxides and hydrocarbons. Up to now the total carbon content has been attributed to carbides and free carbon only. The possible contributions of the other species to the carbon content can be estimated as follows. With a total surface area of 2.1×10^{-5} sites/g cat (see table 3.8), the maximum contribution of carbon oxides (2.5×10^{-4} g/g cat) is a neglectible fraction of the total carbon content. Also no significant contribution to the total carbon content is obtained from a surface that is fully covered with hydrocarbon intermediates (3.6×10^{-4} g/g cat). The latter value is calculated by assuming that the Schulz-Flory distribution is obeyed. The total amount of carbon on the surface is given by:

$$\sum_{n=1}^{\infty} n\, C_n^* = \frac{1}{(1-\alpha)^2}\, C_n^*$$

where C_n^* is the surface coverage of hydrocarbon intermediates with n carbon atoms.
The total surface coverage of hydrocarbon intermediates is given by:

$$\sum_{n=1}^{\infty} C_n^* = \frac{1}{1-\alpha}\, C_1^* = 1$$

A Schulz-Flory constant $\alpha = 0.3$ is taken as a representative value for hydrocarbon synthesis with iron catalysts at the process conditions used. The equations used above can also be applied to estimate the maximum amount of higher hydrocarbons that could condense in the pores of the catalyst. Even if it is assumed that all hydrocarbons with a boiling point equal or higher than the synthesis temperature

Figure 3.15. Scanning electron microscope pictures of an impregnated iron/alumina catalyst before reduction (a and b) and after synthesis (c and d).
(Picture b and d show a enlarged detail of picture a and c, respectively)

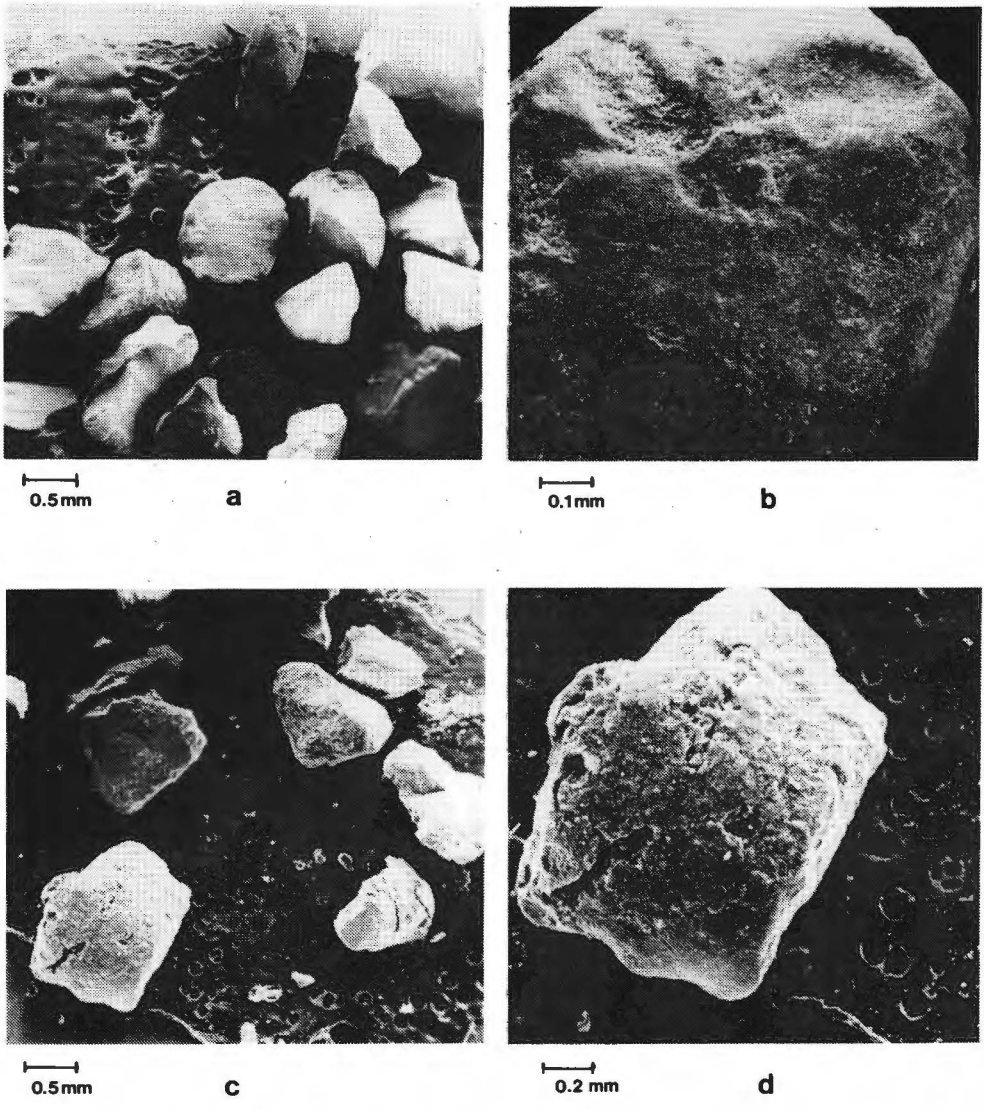

stay on the catalyst and fill its pores, then one can calculate that about 10^{-9} g carbon/g cat will be contributed from higher hydrocarbons to the total carbon content.

3.3.3. Catalyst stability

In the former paragraphs is clearly demonstrated that sulphate additions can be used as a tool to stop the free carbon formation at high synthesis temperatures. Although some concessions must be made to the synthesis activity of the catalyst, no regeneration procedure will be required to burn off the free carbon deposits. Furthermore no desintegration of the catalyst particles will be noticed. Long test runs at 625 K have been performed, in accordance with the procedure described in the experimental section. Three catalysts are selected that, according to the thermogravimetric and carbon analyses, show the least tendency to form free carbon deposits:

1. 19 Fe_2O_3 : 81 Al_2O_3 (C);
2. 80 Fe_2O_3 : 20 ZnO (B) + 16 x 10^{-3} g/g cat $Fe_2(SO_4)_3$;
3. 80 Fe_2O_3 : 20 ZnO (B) + 32 x 10^{-3} g/g cat $Fe_2(SO_4)_3$.

The first two catalysts, tested at 100 kPa and at different CO- and H_2-partial pressures, do not show any deactivation with respect to hydrocarbon production, but the catalysts plug the reactor after approximately 450 ks. Figure 3.15 (c and d) clearly shows the desintegration of the particles of the iron-on-alumina catalyst.

After more than 6.5 Ms of synthesis with the third catalyst at different CO/H_2-ratios at 625 K and at pressures up to 0.6 MPa, no pressure build up or decline in hydrocarbon productivity is noticed. So only the unsupported catalyst with the highest sulphate content is resistent with respect to both deactivation and free carbon deposition.

REFERENCES

1. Büssemeier, B., Frohning, C.P., Cornils, B., Hydrocarbon Process. 55, (11) (1976)
2. Dry, M.E., Singles, T., Boshoff, L.J., Oosthuizen, G.J., J. Catal. 15, 190 (1969)

3. Vannice, M.A., J. Catal. 37, 462 (1975)
4. Anderson, R.B., Catalysis, Vol. IV, P.H. Emmett, Ed., New York, N.Y., 1-371 (1956)
5. Blyholder, G., J. Phys. Chem. 68, 2772 (1964)
6. Vannice, M.A., J. Catal. 50, 228 (1977)
7. Boreskov, G.K., Kinet. Katal. 14, 7 (1973)
8. Sabatier, P., Sendersens, J.B., C.R. Acad. Sci., Paris, 134, 514 (1902)
9. I.G. Farbenindustrie Aktiengesellschaft, British Patent 322,284 (1929)
10. Asboth, K., Österreichisches Patentschrift 171701 (1952)
11. BASF Aktiengesellschaft, Deutsches Patentschrift 922.933 (1955)
12. Union Carbide and Carbon Corporation, US Patent 2,717,259/260 (1955)
13. Österreichisches Stickstofwerke A.G., Österreichisches Pat. 204018 (1958)
14. Union Carbide Corporation, US Patent 2,824,116 (1958)
15. Ruhrchemie A.G., Deutsches Offenlegungsschrift 2518964/982 (1976)
16. Ruhrchemie A.G., Deutsches Auslegeschrift 2536488 (1976)
17. Madon, R.J., Shaw, H., Catal. Rev.-Sci. Eng. 15 (1), 69 (1977)
18. Layng, E.T., US Patent 2,446,426 (1948)
19. Hammer, H., Bittner, D., Erdöl und Kohle-Erdgas-Petrochemie 31, 8 (1978)
20. Schultz, J.F., Karn, F.S., Anderson, R.B., US Bur. Mines, Rep. Invest. 6974 (1967)
21. Enikeev, E.K., Krylova, M.M., Kinet. Katal. 3, 116 (1962)
22. Kishi, K., Roberts, M.W., J. Chem. Soc. Farad. Trans I 71, 1715 (1975)
23. Jolly, S.C., Official Standardized and Recommended Methods of Analysis, Analyt. Meth. Comm., Heffer, W., & Sons Ltd. (1963)
24. Shah, T., Perotta, A.J., Ind. Eng. Chem., Prod. Res. Dev. 15, 2 (1976)
25. Raupp, G.B., Delgass, W.N., J. Catal. 58, 361 (1979)
26. Dwyer, D.J., Somorjai, G.A., J. Catal. 52, 291 (1978)
27. Wentrcek, P.W., McCarty, J.G., Ablow, C.M., Wise, H., J. Catal. 61, 232 (1980)
28. Dry, M.E., Ind. Eng. Chem., Prod. Res. Dev. 15 (1976)
29. Kölbel, H., Giehring, H., Brennstoff Chem. 44, 369 (1963)

30. Kölbel, H., Giehring, H., Brennstoff Chem. 44, 343 (1963)
31. Dry, M.E., Shingles, T., Boshoff, L.J., J. Catal. 25, 99 (1972)
32. Zein El Deen, A., Jacobs, J., Baerns, M., Chem. Reac. Eng.-Houston, ACS Symp., Ser. 65, Am. Chem. Soc., Washington, D.C., 26 (1978)
33. Cooper, B.J., Trimm, D.L., J. Catal. 62, 35 (1980)
34. Baker, R.T.K., Barber, M.A., Harris, P.S., Feates, F.S., Waite, R.J., J. Catal. 26, 51 (1972)

APPENDIX 1

List of definitions

r_{C_n} The rate of formation of hydrocarbons with n carbon atoms (moles/s/g cat).

$r_{C_n^-}$ The rate of the formation of paraffines with n carbon atoms (moles/s/g cat).

$r_{C_n^=}$ The rate of formation of olefines with n carbon atoms (moles/s/g cat).

$r_{T,n}$ The rate of conversion of carbon monoxide to hydrocarbons from C_1 to C_n: $r_{T,n} = \sum_{n=1}^{n} ir_{C_i}$ (moles/s/g cat).

$SC_{1,n}$ The methane selectivity is defined as the rate of conversion of carbon monoxide to methane devided by the rate of CO-conversion to hydrocarbons from C_1 to C_n: $SC_{1,n} = r_{C_1}/r_{T,n}$ (fraction).

OC_n The olefine selectivity is defined as the rate of formation of olefines with n carbon atoms devided by the rate of formation of hydrocarbons with n carbon atoms: $OC_n = r_{C_n^=}/r_{C_n}$ (fraction).

APPENDIX 2

Akzo Chemie B.V. Ketjen catalysts.

Gamma Alumina-006-1.5 E

Testnumber: 26898

Surface area: 190 m^2/g

Chemical composition:

SiO_2	0.59%
Na_2O	0.15%
SO_4	1.9 %
Fe	0.04%

Martinswerk

Boehmiet AlOOH Grade RH6

Primary particle size: 0.01-1 µm

Chemical composition:

SiO_2	0.0005-0.001%
Na_2O	0.000%
SO_4	-
Fe_2O_3	< 0.001%

CHAPTER 4

Reactivity of carbon deposits

4.1. INTRODUCTION

In the previous chapter an attempt has been made to relate the activity of the catalyst to the carbonaceous phases formed during synthesis. A disadvantage of the carbon measurements used in that discussion is that they only give information about total carbon content of the catalyst. The result of a more surface sensitive method to study the carbon deposits is discussed in this chapter. The carbonaceous species at or near the catalyst surface are likely to influence the synthesis activity of catalyst. The interaction of the catalyst with synthesis gas is studied, as well as the disproportionation of carbon monoxide. The study of the carbon monoxide disproportionation is of interest because Biloen et al.[1] showed that certain carbon species deposited are likely to be active in the synthesis of hydrocarbons.

Recent publications of Rabo et al.[2] on nickel-, ruthenium- and palladium-catalysts, and of McCarty et al.[3] on nickel catalysts, have shown that by the Boudouard reaction more than one type of carbon can be deposited on the catalyst surface. In McCarty's paper, the carbon species originating from CO-disproportionation are distinguished by temperature programmed surface reaction (TPSR) with hydrogen. We have applied the same method to various species formed on iron catalysts. It will be shown that these measurements render information with respect to the behavior of the catalyst during the synthesis.

4.2. *EXPERIMENTAL*

The experiments are performed in the combined pulse and continuous flow fixed bed reactor system (II), described in chapter 2. Prior to the experiments, the catalyst is in situ reduced with hydrogen for 58 ks at 625 K.

4.2.1. *The catalyst*

In this study a precipitated iron-zinc oxide catalyst (Fe/ZnO, mol ratio = 2) is used. At the end of this chapter results are presented for this catalyst doped with different amounts of iron sulphate. The behavior of the catalyst during the synthesis has been discussed in chapter 3.

4.2.2. *Carbon deposition*

Carbon is deposited on 0.5 g reduced catalyst by exposure to carbon monoxide or synthesis gas.

Prior to the carbon monoxide adsorption the catalyst is degassed in helium for 1 ks at 625 K. During the carbon monoxide adsorption, aliquots of 0.25 cm^3 CO/He gasmixture (mol ratio = 0.33) are injected in the carrier gas stream and transported to the catalyst at a space-time of W/F = 0.67 kg cat.s.dm^{-3} (N.T.P.). Helium is used as the carrier gas, and the total pressure in the reactor is 0.3 MPa.

When a synthesis experiment is performed, a gasmixture of H_2, CO and He is passed over the catalyst at a unit space-time W/F = 0.36 kg cat.s.dm^{-3} (N.T.P.). The synthesis gas is composed of 20% H_2, 20% CO, and 60% He. The total pressure in the reactor is 0.1 MPa.

4.2.3. *Reaction of hydrogen with carbon deposits*

Both temperature programmed- and isothermal surface reaction experiments are performed.

Temperature programmed surface reaction (TPSR)

After the adsorption, the catalyst is cooled to room temperature in flowing helium. Thereafter the helium gas stream over the catalyst bed is switched to pure hydrogen, and the temperature of the catalyst bed is increased at a rate of 0.017 $K.s^{-1}$ from 300 K to 625 K. The space-time of the hydrogen feed is W/F = 0.67 kg $cat.s.dm^{-3}$. The TPSR is carried out at 0.3 MPa.

Isothermal surface reaction (ISR)

After the deposition, the catalyst is flushed with helium, and subsequently cooled to the desired temperature. When the temperature is obtained, the helium gas stream over the catalyst bed is switched to a mixture of hydrogen and helium (space-time W/F = 0.36 kg $cat.s.dm^{-3}$ (N.T.P.)). The standard time interval between the end of the carbon deposition and the start of the surface reaction is 0.3 ks. The deposition and the reaction with hydrogen is carried out at 0.1 MPa.

4.3. RESULTS AND DISCUSSION

4.3.1. Reactivity of carbon species deposited by CO-adsorption

In the first experiments of this series, freshly reduced catalysts are saturated with carbon monoxide at different temperatures by admitting about 20 pulses CO/He. Below 550 K no carbon dioxide is detected in the effluent stream. After completed adsorption, the catalyst is cooled to room temperature. At this temperature the helium carrier stream is switched to pure hydrogen, and the temperature program is started. The reactivity of the carbonaceous species towards hydrogen is recorded as a function of the temperature. The data depicted in figure 4.1 (curve a and b), show that the reactivity of the adsorbed species towards hydrogen is independent of the adsorption temperature, but they also show that the quantity adsorbed does depend on the adsorption temperature. This species is denoted henceforth as α-carbon, albeit possible that this species still contains oxygen.

Figure 4.1. TPSR with hydrogen of carbon containing species deposited by CO-adsorption on freshly reduced Fe/ZnO at different temperatures.

Curve a: saturated deposition at 300 K (1.6×10^{-5} mol C/g cat).

Curve b: saturated deposition at 500 K (8.0×10^{-5} mol C/g cat).

Curve c: 6 pulses CO at 550 K.

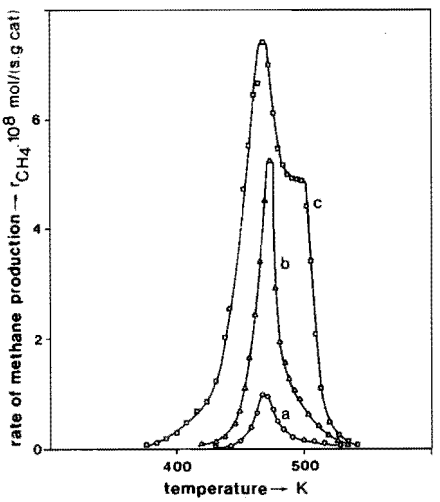

Increasing the temperature to 550 K, CO_2 is detected in the effluent stream during CO-adsorption. The results of a TPSR-experiment performed after adsorbing a limited amount of six pulses CO at 550 K, as depicted in figure 4.1 (curve c), suggest that two different species contribute to the observed methane production.

When a freshly reduced catalyst is saturated with carbon monoxide at room temperature, and thereafter heated to 475 K and cooled again to room temperature, an additional quantity of carbon monoxide is adsorbed when CO is admitted again. The TPSR-data show, that even when a catalyst is treated with five consecutive CO-adsorptions with intermediate heating/cooling cycles, only α-carbon is formed. The total methane production amounts to 0.037 mmol.g cat^{-1} while after one CO-adsorption 0.016 mmol.g cat^{-1} methane is formed upon TPSR.

Figure 4.2. TPSR with hydrogen of carbon containing species deposited by CO-adsorption on freshly reduced Fe/ZnO at 515 K.
Curve a: catalyst immediately cooled to room temperature after deposition.
Curve b: catalyst cooled to room temperature 3.6 ks after deposition.

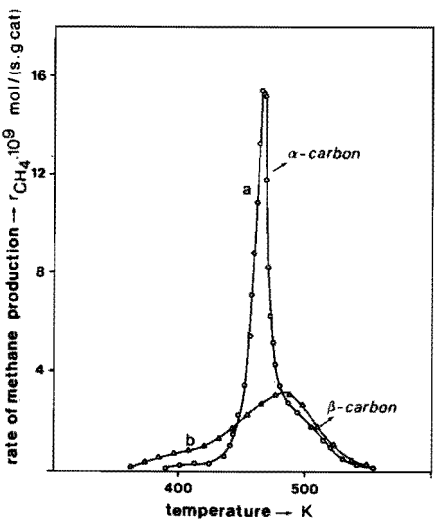

The α-carbon species deposited by CO-adsorption at 515 K is not stable at this temperature. Figure 4.2, curve a shows the results of the TPSR-experiment, when the catalyst is cooled to room temperature immediately after two CO-pulses have been passed over the catalyst at 515 K. When after admitting the two carbon monoxide pulses the catalyst is held at 515 K for 3.6 ks, the TPSR-data show that a part of the α-carbon is transformed to a species with a lower reactivity towards hydrogen (figure 4.2, curve b). The latter species is referred to as β-carbon.

Figure 4.3 shows the result of two TPSR-experiments with the same catalyst. Curve a represents the data of the surface reaction of a freshly reduced catalyst, which is saturated with carbon monoxide at 300 K. Here 0.018 mmol.g cat^{-1} methane is formed, and the species is identified as α-carbon. When immediately after the temperature of 625 K is reached in the TPSR experiment, the catalyst is cooled to

Figure 4.3. TPSR with hydrogen of carbon containing species deposited by CO-adsorption at room temperature on Fe/ZnO.
Curve a: deposition on a freshly reduced catalyst.
Curve b: deposition on a used catalyst.

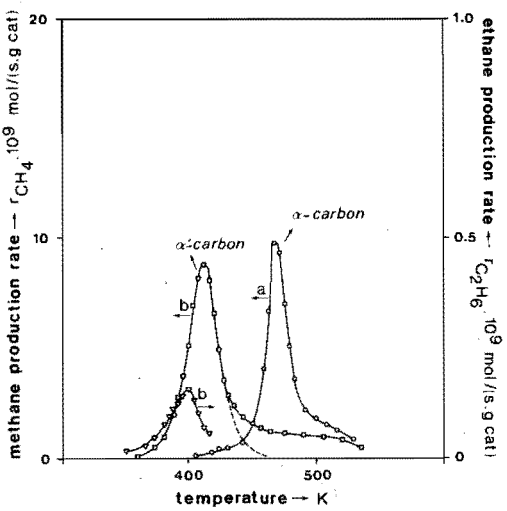

room temperature, and again contacted with CO the TPSR results (curve b) show that a species is formed that is much more reactive towards hydrogen. The peak maximum in the rate of methanation is shifted from about 470 to 410 K. Whereas from α-carbon only methane is found in TPSR, the highly reactive carbon species yields methane and ethane. In analogy with McCarty et al.[3], this reactive species is designated as α'-carbon. The amount of α'-carbon hydrogenated after saturated CO-adsorption at 300 K is 0.016 mmol.g cat^{-1}. When a room temperature CO-adsorption/TPSR experiment is performed with a catalyst that is used in a previous experiment in which carbon monoxide is adsorbed at 500 K, more α'-carbon is deposited (0.045 mmol.g cat^{-1}), as is illustrated in figure 4.4. Apart from the α'-carbon, also an appreciable amount of another type of carbon is formed on the used catalyst. This carbon species hydrogenates at higher temperatures, and closely resembles the reduction characteristics of β-carbon, formerly identified by TPSR after prolonged heating of α-carbon at 515 K.

Figure 4.4. TPSR with hydrogen of carbon containing species deposited by CO-adsorption at room temperature on Fe/ZnO. Prior to the experiment the catalysts were used in a 300 K-CO-adsorption/TPSR-experiment (curve a) and a 500 K-CO-adsorption/TPSR-experiment (curve b).

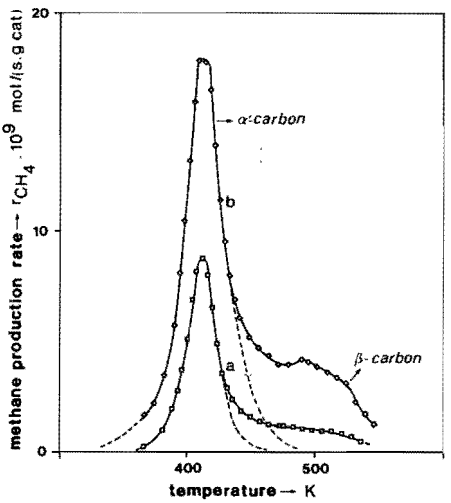

In a subsequent series of experiments it is shown that a used catalyst requires an intensive reduction treatment to regain the adsorption properties towards CO shown by the virgin catalyst. A freshly reduced catalyst is saturated with carbon monoxide at room temperature. The α-carbon deposits are reduced by TPSR with hydrogen. Thereafter, the catalyst is reduced in hydrogen at 625 K for 58 ks, degassed in helium for 1 ks and cooled down to room temperature. After this procedure, the CO-adsorption at room temperature and again TPSR showed the normal quantity of 0.012 mmol.g cat^{-1} α-carbon. At the end of the TPSR experiment, the hydrogen is switched to helium and the catalyst is held at 625 K for 58 ks. Thereafter, the catalyst is cooled down to room temperature and a CO-adsorption/TPSR experiment is performed. Here, α'-carbon and β-carbon are the only species that contributes to the methane formation. The amount of α'-carbon hydrogenated is 0.016 mmol.g cat^{-1}.

4.3.2. The role of carbon species in the synthesis

Two experiments were performed to clarify the significance of the different carbon species for the hydrocarbon synthesis. In both experiments the catalyst is activated in a continuous flow of synthesis gasmixture at 550 K. When the maximum synthesis activity is obtained, the gas stream is switched to helium. In the first experiment after 0.3 ks the gas flow is switched from helium to hydrogen at 550 K. In the second experiment the catalyst is rapidly cooled to room temperature in helium, and the temperature program is started after the helium is switched to hydrogen. The results of the ISR- and the TPSR-experiment are shown in figure 4.5 and 4.6 respectively. Figure 4.5 shows three stages in the reduction of carbon. In the first stage both the methane and the ethene production decrease as the reduction time proceeds. Apart from methane and ethene also small amounts of water are observed at the beginning of the ISR experiment. After this

Figure 4.5. Activation of a Fe/ZnO catalyst at 550 K (curve a: methane formation)($x_{H_2} = x_{CO} = 0.2$), and reduction with hydrogen of the carbonaceous species deposited over this period at 550 K (curve b: methane formation; curve c: ethane formation)($x_{H_2} = 1.0$).

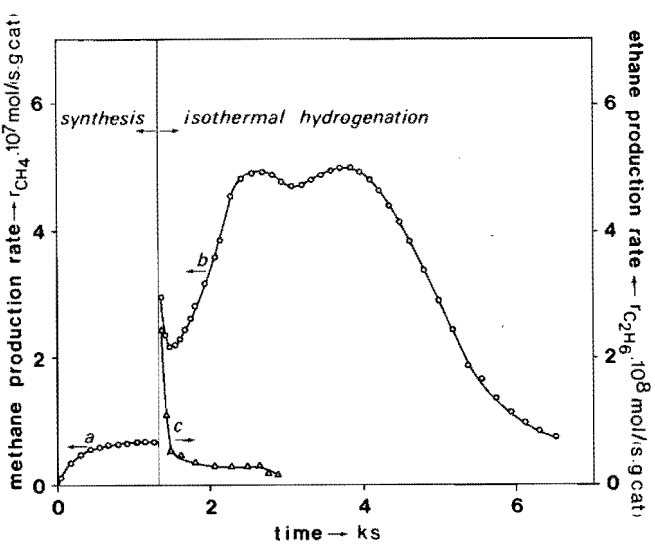

Figure 4.6. Temperature programmed reduction with hydrogen of carbonaceous species deposited during the synthesis at 550 K (curve a: methane formation; curve b: enlarged version of curve a).

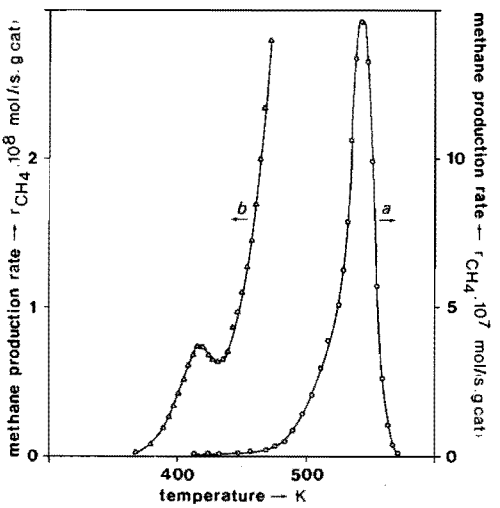

first period the rate of methane formation is found to increase and then to decrease again, but the ethane production does not increase correspondingly. In the third stage an autocatalytic effect similar to the second stage is noticed, but no ethane can be detected any more. Evidently three types of carbon are detected in this experiment. The carbon reduced in the first stage is readily accessible for hydrogen, and higher products can be formed from this carbon species. At the start of the reduction the second and third stage carbon are not yet or to a small amount reactive towards hydrogen. It is probable that the first stage carbon species plays an important role in the synthesis of hydrocarbons, and it is not improbable that this species in fact is the most abundant surface species that determines the synthesis activity of the catalyst and that the activation of iron catalysts means the formation of this species. Figure 4.6 curve b shows that the most reactive surface species has a peak maximum in the methanation at about 415 K. This temperature of maximum methanation rate strongly resembles the peak temperature in the TPSR of

α'-carbon discussed in the former paragraph, and this type of carbon is undoubtedly the same as the first stage carbon species in figure 4.5.

When we look at the quantities of hydrocarbons formed, it is possible to distinguish surface and bulk carbon species. The total amount of carbonaceous species detected during the isothermal reduction experiment is about 1.8 mmol/g cat. Resolution of the α'-carbon peak from figure 4.6 shows that 0.02 mmol carbon/g cat is present in the α' found. The amount of carbon assigned to α'-carbon in figure 4.5 amounts to 0.03 mmol/g cat. The latter two data are in the order of one monolayer (0.02 mmol/g cat). The excess 1.8 mmol/g cat has to be apportioned to subsurface- or bulk carbon species.

4.3.3. Reactivity of carbonaceous material deposited during the synthesis

The autocatalytic behavior of the hydrogenation of carbon, noticed in the previous paragraph, is also observed by several authors[4,5]. Rosinski and coworkers[5] described the kinetics of this reaction with a model frequently used to explain the kinetics of topochemical reactions. The physical picture behind this model is that nuclei of the solid phase reaction product are formed through contact with the reactant gas, and further reaction is largely localized on an interface between the solid reactant and the solid product. The interfacial area changes with the passage of time. According to the model three different stages in the kinetics of the process can be distinguished. The first stage is an induction period for the relative slow formation of nuclei in the solid product phase. In the second stage, the reaction rate increases, because nuclei not only form but also grow, thereby increasing the interface between the solid phases. The individual nuclei fuse in the third stage of the process, thereby reducing the interfacial area and the reaction rate.

The rate of the reaction between hydrogen and carbonaceous material deposited on the catalyst, will be a function of the fraction converted (X), the gasphase hydrogen concentration (H_2), and the temperature.

Hence:

$$dX/dt = F\ (T,H_2,X) \qquad (4.1)$$

When, in the model described above, the dependencies of the rate of nucleation and of nucleus growth of the different carbonaceous deposits on the temperature and hydrogen pressure are the same, the area of the interface between the solid phases is independent of the process conditions at a fixed degree of reaction and can then be written in power law form as:

$$(dX/dt)_X = k_0 \exp(-E_a/RT) \quad (H_2)^a \tag{4.2}$$

To test the validity of equation (4.2), hydrogenation experiments are carried out with five different partial pressures of hydrogen at 550 K, and with four different temperatures in pure hydrogen. Prior to the hydrogenation experiment a synthesis gasmixture ($x_{H_2} = x_{CO} = 0.2$) is passed over the freshly reduced catalyst at 550 K for 240 s. After the synthesis period the synthesis gasmixture is switched to helium and the reactor temperature is adjusted to the required surface reaction temperature. A fixed period of 0.3 ks is maintained between the synthesis and the reduction experiment. Figures 4.7 and 4.8 show the dimensionless reaction rates as a function of the degree of conversion. Evidently the shape of the curves is independent of

Figure 4.7. Hydrogenation of carbonaceous material deposited during 240 s of synthesis at 550 K on Fe/ZnO. Different partial pressures of hydrogen (T = 550 K).

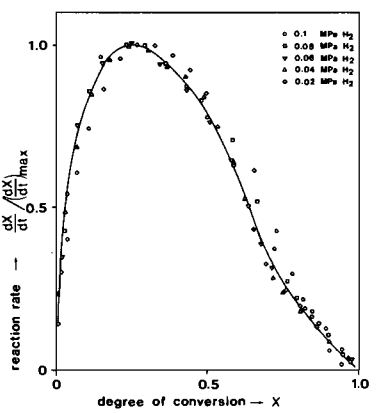

Figure 4.8. Hydrogenation of carbonaceous material deposited during 240 s of synthesis at 550 K on Fe/ZnO. Different hydrogenation temperatures (x_{H_2} = 1.0).

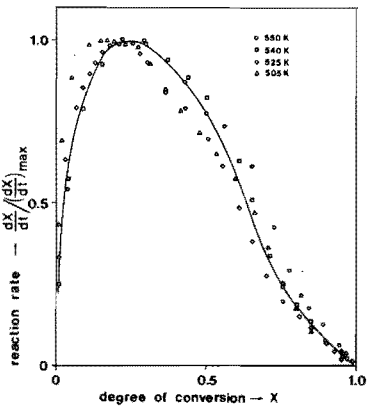

the partial pressure of hydrogen and of the temperature, within experimental error. This proves that the reaction rate can be described in the power law form (equation 4.2). The temperature and hydrogen partial pressure dependency of the reaction rate can now be calculated according to equation 4.2 at a fixed degree of conversion. The

Figure 4.9. Rate of methane production at maximum reaction rate as a function of hydrogen partial pressure and of temperature.

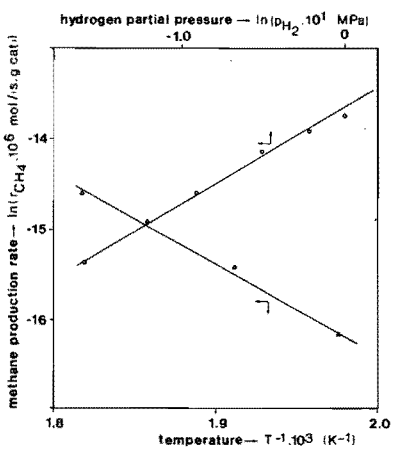

reaction rate at the top of the curve is depicted as a function of the hydrogen partial pressure and the temperature in figure 4.9. From this graph an order in hydrogen of 1.0, and an apparent activation energy of 82 kJ/mol is calculated.

For the dependency of the reaction rate on the degree of conversion, Bond[6] derived the following equation for the relation between the degree of reduction and the time.

$$dX/dt = (k/(2\ X_i))\ (1 - 2\ X_i + X)\ (1 - X) \qquad (4.3)$$

where: dX/dt = rate of reaction;

X = fraction converted;

k = specific rate constant;

X_i = fraction converted at the maximum reaction rate, when the maximum rate is obtained between $0 < X < 0.5$.

Figure 4.10. Hydrogenation of carbonaceous material deposited during 240 s of synthesis at 550 K on Fe/ZnO.
Curve a : hydrogenation at 550 K; $x_{H_2} = 1.0$.
Curve b : hydrogenation at 550 K; $x_{H_2} = 0.6$.
Curve b_1: calculated contribution of the most reactive carbonaceous species; $x_{H_2} = 0.6$ (I).
Curve b_2: calculated contribution of the second type of carbonaceous material; $x_{H_2} = 0.6$ (II).

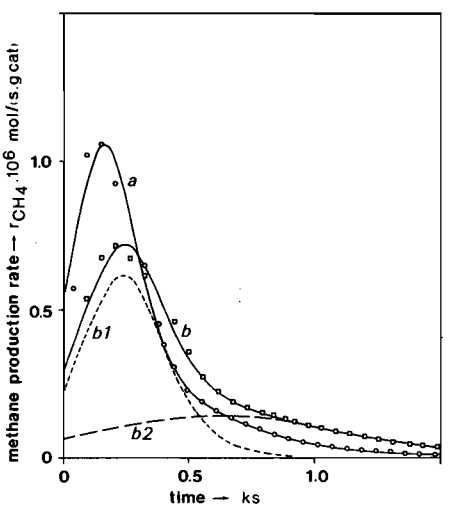

Because the reduction of carbonaceous material from an iron catalyst used for approximately 1 ks at 550 K in the synthesis (figure 4.5), shows two autocatalytic stages, two different types of carbon are allowed in this model to describe the experimental data. Details of the solution method are given in appendix 3 at the end of this chapter. The solid lines in figure 4.10 are calculated according to the integrated form of equation 4.3. It can be seen that a reasonable agreement exists between the rates measured experimentally, and the rates calculated with the model in which two types of carbon are permitted. The individual contributions of the two types of carbon are presented by the broken lines in figure 4.10.

Figure 4.11. Hydrogenation of carbonaceous material deposited during different synthesis periods at 550 K on Fe/ZnO. Hydrogenation at 550 K and $x_{H_2} = 1.0$.

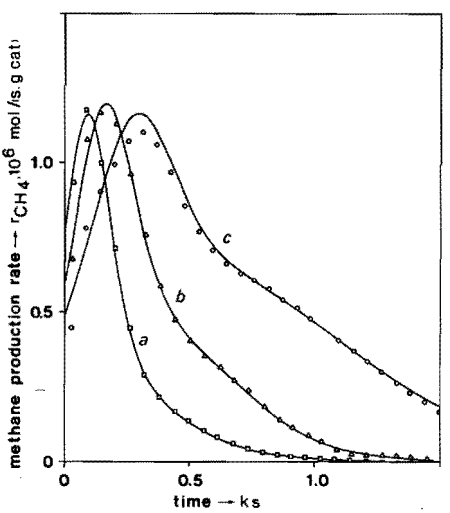

Kinetic parameters (C_o = carbon content (mol/g cat); x_i = fraction converted at the maximum reaction rate; k = specific reaction rate constant).

		CARBONACEOUS SPECIES I			CARBONACEOUS SPECIES II		
		C_o	x_i	k	C_o	x_i	k
curve a	after 120 s synthesis	2×10^{-4}	0.37	9×10^{-3}	1×10^{-4}	0.38	4×10^{-3}
curve b	after 240 s synthesis	3×10^{-4}	0.42	8×10^{-3}	2×10^{-4}	0.46	4×10^{-3}
curve c	after 480 s synthesis	3×10^{-4}	0.45	7×10^{-3}	7×10^{-4}	0.43	2×10^{-3}

The build up of carbonaceous material during the synthesis is also studied by isothermal surface reaction. The catalyst is exposed to synthesis gas ($x_{H_2} = x_{CO} = 0.2$) for a specified period at 550 K, and thereafter the ISR experiment is performed at the same temperature. Figure 4.11 shows the result of the hydrogenation of carbonaceous material deposited during the different synthesis periods. The lines represent the result of the rates estimated by the least square method using the experimental data and the model described above. The values of the kinetic parameters obtained from these calculations are also shown in figure 4.11. In terms of carbon built up during the synthesis, the results show, that initially a carbon species is formed that is quite reactive towards hydrogen. The reactivity of this carbon species decreases with time-on-stream, and a second carbonaceous phase is formed. The decrease in reactivity due to aging of the carbon species initially formed during the synthesis is shown in figure 4.12. In this figure, curve a represents the methane production of a catalyst exposed to hydrogen after a synthesis period of 240 ks. Curve b shows the data of the hydrogenation experiment with the same catalyst exposed to synthesis gas for 240 s, only the carbon species are aged for 58 ks at 550 K in flowing helium before the reduction is started.

Figure 4.12. Hydrogenation of carbonaceous deposits formed during 240 s of synthesis at 550 K on Fe/ZnO.
Curve a: hydrogenation is started 0.3 ks after the synthesis is stopped.
Curve b: hydrogenation is started 58 ks after the synthesis is stopped.

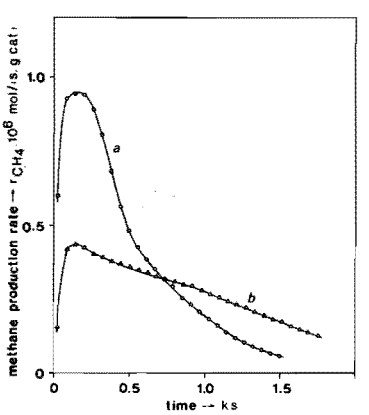

4.3.4. Influence of sulphate on the reactivity of carbon species

Three freshly reduced catalysts containing 0, 0.003 and 0.03 weight fraction $Fe_2(SO_4)_3$ are exposed to synthesis gas ($x_{H_2} = x_{CO} = 0.2$). For the first two catalysts the synthesis is stopped when the maximum activity is obtained. The temperatures at which these catalysts are activated are 550 K and 625 K, respectively. The third catalyst is activated in the synthesis for 3.6 ks at 625 K. At the end of the synthesis period, the catalysts are cooled in helium to room temperature, and thereafter a TPSR experiment is started. Because the most reactive carbon species are of interest with respect to the synthesis activity of the catalyst, these are the only ones depicted in figure 4.13 as a result of the TPSR experiment.

Figure 4.13. Temperature programmed reduction with hydrogen of carbonaceous material deposited during the synthesis ($x_{H_2} = x_{CO} = 0.2$) on Fe/ZnO.
Curve a: synthesis at 550 K; $x'_{Fe_2(SO_4)_3} = 0.000$.
Curve b: synthesis at 625 K; $x'_{Fe_2(SO_4)_3} = 0.003$.
Curve c: synthesis at 625 K; $x'_{Fe_2(SO_4)_3} = 0.03$.

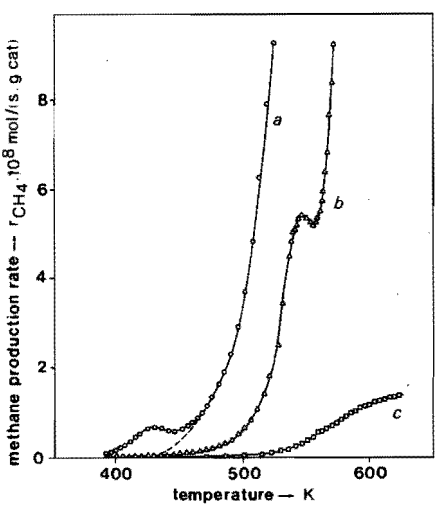

4.4. *CONCLUSIONS*

4.4.1. *Reactivity of carbon species deposited by CO-adsorption*

By CO-adsorption on the iron catalyst studied, at least three different carbonaceous species are formed. These types are distinguished by their reaction with hydrogen. Results reported in the literature, show that the interaction of carbon monoxide with different iron substrates is dissociative at room temperature[7-10]. In chapter 3 (table 8) it is shown that the amount of carbon monoxide adsorbed at room temperature corresponds to the quantity of hydrogen adsorbed. Since hydrogen is known to adsorb dissociatively, we conclude that the products of CO-adsorption stay on the surface at room temperature (on top adsorption). When CO is adsorbed at higher temperatures, the amount of carbon monoxide adsorbed on the catalyst surpasses the monolayer coverage. Evidently the carbon and oxygen adspecies can dislodge the lattice atoms from their equilibrium position and cause rearrangements in the top layers of the catalyst. This reconstruction indicates the formation of chemical bonds between the adsorbed atoms and the substrate, and may be looked upon as a two dimensional precursor for the oxide and carbide formation. Textor et al.[11] reported the formation of such a carbide-oxide-layer upon CO adsorption at room temperature on a α-Fe(111)-single crystal surface. The carbon species in this carbide-oxide-layer are denoted in the former paragraphs as α-carbon.

The formation of β-carbon during temperature treatment of α-carbon at 550 K can be explained by a further chemical reaction in which the subsurface species are allowed to diffuse into the bulk, where a three dimensional iron/carbon layer is formed, possibly by segregations into isolated iron-carbon and iron-oxygen areas.

When the carbon/oxygen layer is removed by TPSR, the characteristics of the catalyst have changed with respect to the freshly reduced catalyst. The toplayers remain reconstructed under normal TPSR conditions. Only prolonged reduction with hydrogen at 625 K can regenerate the catalyst to its virgin state. Apparently, relaxation of the rearranged toplayers is inhibited by small amounts of carbon or oxygen impurities in the catalyst, that are left after the TPSR experiment. That some type of reducible impurities is required is shown by

the observation that prolonged heating in the helium atmosphere leaves the catalyst in its reconstructed form. That we have only a small quantity of impurities follows from the observation that within experimental error, the amount of carbon monoxide adsorbed on the virgin catalyst is balanced by the amount of methane formed during the TPSR experiment. When CO is adsorbed again on the reconstructed reduced surface, α'-carbon is formed together with a carbon structure that strongly resembles β-carbon, ascribed to a three dimensional carbon/iron structure. On top of this β-carbon containing structure, α'-carbon is stabilized. Following this line of argument α'-carbon species have to be attributed to surface carbon species. The amount of α'-carbon and of β-carbon species formed upon CO-adsorption on the used catalyst depends on the extent of reconstruction. High CO-adsorption temperatures on a freshly reduced catalyst favour a high extent of reconstruction, thereby increasing the surface area of the catalyst. This increased surface area is shown by an increased capacity for α'-carbon of the reconstructed catalyst.

In summary, the results discussed this far show that the carbonaceous deposits formed by CO-adsorption are species that are localized in subsurface layers. The formation of these layers reconstruct the top layers of the catalyst. When the deposits are hydrogenated methane is the only product detected. After hydrogenation under normal conditions, the reconstruction of the catalyst is maintained. Two types of carbonaceous species are formed when CO is adsorbed on a reconstructed surface: surface carbon containing species, that, apart from methane, also forms ethane upon hydrogenation, and a three dimensional carbide-like structure.

A number of authors show that the formation of different types of carbonaceous species by carbon monoxide adsorption are not restricted to iron only. On nickel Rabo et al.[2] report that the carbon deposits formed by CO-dissociation can react with hydrogen to hydrocarbons at room temperature. However, the amount that reacts at room temperature with hydrogen is only a small fraction of the total amount of carbon deposited. The carbon deposits become less reactive after heat treatment at 775 K. McCarty et al.[3] have characterized three types of carbon on alumina supported nickel catalysts. The most abundant species formed upon CO-dissociation are described as chemisorbed carbon atoms (α-phase) and amorphous carbon (β-phase). At low

coverage a very reactive α'-phase is detected. The α-carbon species can be transformed to β-carbon upon temperature treatment at about 600 K.

Araki and Ponec[12] show that nickel substrates can be modified by a synthesis gasmixture. Starting with a virgin nickel film, the initial activity of methane formation becomes progressively higher in successive runs. Between the runs the film is reduced with hydrogen at 575 K. The increased initial activity could be ascribed to an increased amount of the most reactive surface species (α'-carbon) formed on the modified catalyst.

4.4.2. The role of carbon species in the synthesis

The study most closely related to the results presented here on the different carbonaceous species formed during the synthesis, is published by Matsumato and Bennett[13]. The authors applied the transient method to study the synthesis over fused iron catalysts. It was found that when the reaction mixture is suddenly changed to hydrogen, after the steady state is obtained, the methane production first increases and then decreases with time-on-stream. The total amount of carbon flushed off in this first period is in the order of a monolayer, and called by them X-carbon. When after this first period the temperature is increased to 675 K, a total amount of 5.7 mmol CH_4.g cat^{-1} is produced. This amount corresponds to a stoichiometry of $Fe_{2.2}C$. In agreement with our results, the species that is hydrogenated in the first period is postulated as the active surface species in the synthesis. The X-carbon is the most reactive species towards hydrogen, and apart from methane, also ethane and propane are formed upon hydrogenation of this carbon species.

4.4.3. Reactivity of carbonaceous material deposited during the synthesis

When the catalyst is exposed to hydrogen after the synthesis is stopped at the maximum hydrocarbon production rate, two types of bulk carbon species are identified (figure 4.5). These two types of carbon are also observed on fused iron catalysts by Rosinski et al.[5]. The first most reactive type of bulk carbon is transformed to a less

reactive species after prolonged heating at 550 K, as is illustrated in figure 4.12. Because χ-Fe_5C_2 and ε-$Fe_{2.2}C$ are known to be the stable carbides at the temperature used[14,15], the first type of bulk carbon can only be an intermediate carbide structure. A carbide structure between α-Fe and the stable carbides is reported by Niemantsverdriet et al.[15]. This intermediate carbide (Fe_xC) is converted to the stable carbides in the course of the synthesis.

4.4.4. Influence of sulphate on the reactivity of carbon species

Figure 4.13 shows that the reactivity towards hydrogen of carbon species deposited during the synthesis decreases when the amount of sulphate on the catalyst increases. The same behavior is noticed by Wentrcek et al.[16] with a Ni/Al_2O_3 catalyst poisoned with H_2S. These authors find, that the amount of carbon that can be converted to methane by pulses of hydrogen at 555 K decreases as the H_2S loading of the catalyst increases. The decreased hydrogenation activity is explained by assuming a rapid conversion of surface carbon species to a less reactive form under the influence of sulphur. If this explanation would be correct in the case of the sulphate poisoned iron catalysts, it would be expected that the α'-carbon species are converted to a less reactive form during synthesis, and that consequently the results of the TPSR experiments would fit the dashed curve in figure 4.13. In the case of iron the results (curve b) imply that also at least two kinds of carbonaceous species are formed on sulphate promoted iron catalysts, but that the reactivity of these species towards hydrogen is decreased when the sulphate content is increased.

REFERENCES

1. Biloen, P., Helle, J.N., Sachtler, W.H.M., J. Catal. 58, 95 (1979)
2. Rabo, J.A., Risch, A.P., Poutsma, M.L., J. Catal. 53, 295 (1978)
3. McCarty, J.G., Wise, H., J. Catal. 57, 406 (1979)
4. Raupp, G.B., Delgass, W.N., J. Catal. 58, 361 (1979)

5. Rozovskii, A.Ya., Ivanov, A.A., Kagan, Yu.B., Bashkirov, A.N., Kinet. Katal. 4, 97 (1963)
6. Bond, W.D., J. Am. Chem. Soc. 66, 1573 (1962)
7. Yu, K.Y., Spicer, W.E., Lindau, I., Pianetta, P., Lin, S.F., Surf. Sci. 57, 157 (1976)
8. Ertl, G., Küppers, J., Nitschke, F., Weiss, M., Chem. Phys. Lett. 52, 309 (1977)
9. Kishi, K., Roberts, M.W., J. Chem. Soc. Farad. Trans I 71, 1715 (1975)
10. Perrichon, V., Primet, M., Nahon, N., Turlier, P., C.R. Acad. Sci. Paris, C289, 149 (1979)
11. Textor, M., Gray, I.D., Mason, R., Proc. R. Soc. London, A356, 37 (1977)
12. Araki, M., Ponec, V., J. Catal. 44, 439 (1976)
13. Matsumoto, H., Bennett, C.O., J. Catal. 53, 331 (1978)
14. Raupp, G.B., Delgass, W.N., J. Catal. 58, 348 (1979)
15. Niemantsverdriet, J.W., v.d. Kraan, A.M., v. Dijk, W.L., v.d. Baan, H.S., J. Phys. Chem., in press
16. Wentrcek, P.W., McCarty, J.G., Ablow, C.M., Wise, H., J. Catal. 61, 232 (1980)
17. Marquardt, D.W., J. Soc. Ind. Appl. Math. 11, 431 (1963)

APPENDIX 3

When the maximum rate of an autocatalytic reaction occurs before 50 percent of the solid reactant is converted, Bond[6] derived equation 4.4.

$$dX/dt = (k/(2\ X_i))(1 - 2\ X_i + X)(1 - X) \qquad (4.4)$$

where: dX/dt = rate of reaction;

X = fraction converted;

k = specific rate constant;

X_i = fraction converted at the maximum reaction rate.

Integration of 4.4 gives:

$$\ln((1 - 2\ X_i + X)/(1 - X)) = ((1 - X_i)/X_i)(kt + C) \qquad (4.5)$$

where:

$$C = (X_i/(1 - X_i))\ \ln(1 - 2\ X_i) \qquad (4.6)$$

when $X = 0$ at $t = 0$.

Substituting equations 4.5 and 4.6 in equation 4.4 gives:

$$dX/dt = \frac{A\ B\ (1 + A)\ \exp(Bt)}{((1 + A\ \exp\ (Bt))^2} \qquad (4.7)$$

where: $A = 1 - 2\ X_i$ and $B = k(1 - X_i)/X_i$.

Because dX/dt equals $dCH_4/C_o dt$, where C_o is the initial carbon concentration and dCH_4/dt is the rate of methane production, the methane formation as a function of time can be given by:

$$dCH_4/dt = \frac{D\ \exp(Bt)}{(1 + A\ \exp(Bt))^2} \qquad (4.8)$$

where $D = C_o\ A\ B\ (1 + A)$.

Two solutions are possible for equation 4.8, but one solution only has physical significance. The relation between the two solutions are: $A = 1/A'$, $B = -B'$, $D = D'A'^2$. The relation between the constants A, B, and D and the values for X_i, k and C_o are:

$$X_i = (1 - A)/2$$

$$k = (X_i/(1 - X_i))\ B$$

$$C_o = D/(A\ B\ (1 + A))$$

From equation 4.8 the best estimates of the unknown parameters A, B, and D have been calculated with an Algol 60 program, which is developed by the Mathematical Department of the University of Technology of Eindhoven. This program is derived from a general procedure based on the Marquardt algorithm[17].

The assumption required to solve the equation proposed by Bond is that the degree of reduction is zero at the start of the reduction. Since the rate of reduction depends on the carbide concentration, the initial segment of the kinetic curve can in principle depend on the carbon content of the catalyst. In that case the starting condition (4.6) would not be met. However, Rosinski et al.[5] have found that the initial segment of the kinetic curve is independent of the amount of carbon, and they have concluded that the carbon content of the surface layers has to be close to 100 percent. The results of the solution as depicted in figure 4.11, give a further justification: The calculated degrees of conversion at maximum reaction rate is reasonably independent of the time of synthesis.

CHAPTER 5

Kinetics of the Fischer-Tropsch synthesis

5.1. INTRODUCTION

According to the International Union of Pure and Applied Chemistry (IUPAC[1]) the turnover frequency of a catalytic reaction is defined as the number of molecules reacting per active site in unit time. The term active site is applied to those sites for adsorption which are effective sites for a particular heterogeneous catalytic reaction. Because it is often impossible to measure the amount of active sites, some indirect method is needed to express the rate data in terms of turnover frequencies. In some cases a realistic measure of the number of active sites may be the number of molecules that can be adsorbed of some compound. This measure is frequently used in the literature of the Fischer-Tropsch synthesis, where the amount of adsorption sites is determined by carbon monoxide adsorption on the reduced catalyst. However, this result is only applicable to the determination of the turnover frequency if the number of adsorption sites on the reduced catalyst is really an indication of the amount of active sites on the catalyst during the synthesis, and especially for the Fischer-Tropsch synthesis with iron catalysts this method is questionable. Not only is the reduced α-iron phase converted to iron carbide, but also the amount of CO adsorbed depends on the pretreatment of the catalyst. The latter phenomenon has been discussed in the previous chapter.

The turnover frequencies reported in the literature are small. In the publication of Vannice[2] the turnover frequencies for CO-conversion

to hydrocarbons range from 0.325 s^{-1} for ruthenium to 0.002 s^{-1} for iridium at 550 K and 0.1 MPa. At the same process conditions, for iron a value of 0.16 s^{-1} is given.

Dautzenberg et al.[3] have determined the kinetics of the Fischer-Tropsch synthesis with ruthenium catalysts. The authors showed, that because the synthesis can be described by a consequetive mechanism, the transient behavior of the catalyst can give information about the kinetics of the process. On ruthenium they found that not only the overall rate of hydrocarbon production per active site is small, but also that the rate constants of propagation and termination are low.

Our doubts about the published low rates of a number of reaction steps in the synthesis, initiated research to get first-hand information about the rate of these steps. In this study the transient method is applied to iron catalysts.

5.2. CALCULATION BASIS FOR PULSE SIMULATION

Since the results that will be reported in this paragraph will be strongly related to the work of Dautzenberg et al. their nomenclature will be used.

To be able to describe the kinetics of the synthesis, the mechanism of the reaction has to be clear. Although there is no common agreement about the details of the reaction mechanism, a number of features are generally accepted:

- the reaction is initiated by mono-carbon species;
- the chain growth takes place by a stepwise addition of monocarbon units to the growing chain;
- the rate of termination and the rate of propagation are independent of the chain length.

According to these simplifying assumptions the general scheme of the reaction can be given by:

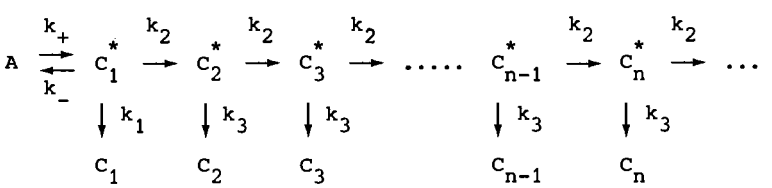

Where: C_n^* is a hydrocarbon surface intermediate with n carbon atoms;
C_n is the hydrocarbon product with n carbon atoms;
A is the precursor for the initiating species;
k_1, k_2, k_3 are the rate constants for methane termination, and propagation, and termination of higher hydrocarbons, respectively.

Because, in most cases, the production of methane does not obey the Schulz-Flory distribution, the rate constant of methane termination (k_1) is allowed to differ from k_3. The Schulz-Flory constant is defined as:

$$\alpha = \frac{dC_n/dt}{dC_{n-1}/dt} \qquad (5.1)$$

A number of mechanisms are claimed to describe the propagation step. These mechanisms are:
- chain growth by condensation of oxygen containing species;
- chain growth by carbon monoxide insertion into the metal-hydrocarbon bond;
- chain growth by polymerization of oxygen free CH_x-species.

For all these mechanisms the propagation reaction can be expressed as:

$$C_{n-1}^* + C_1^{**} \longrightarrow C_n^{**}$$

where C_1^{**} is the building block for the hydrocarbon chains. With respect to the propagation mechanisms presented, a number of possibilities arise for the status of C_1^{**}. For CO-insertion, C_1^{**} will either be the precursor (A) for the initiating species, or it may be a precursor for A. In the first case C_1^{**} = A, in the latter case it is reasonable to assume that C_1^{**} is in equilibrium with A, hence $[C_1^{**}] = K[A]$. For condensation, C_1^{**} is identical to C_1^*, but for polymerization C_1^{**} need not be identical to C_1^*. However, in the case that C_1^{**} is not identical to C_1^*, the building block is either a precursor for C_1^*, or a hydrogenated form of C_1^*. In the first case C_1^{**} = A. For the second case, it is assumed here that C_1^{**} and C_1^* are in equilibrium, hence $[C_1^{**}] = K[C_1^*]$.

The rate equations that have to be solved for the different models are:

- For the CO-insertion model, and the polymerization model (where $C_1^{**} = A$)

$$dC_1/dt = k_1[C_1^*]$$

$$d[C_1^*]/dt = k_+[A] - (k_2[A] + k_1 + k_-)[C_1^*] \qquad (5.2)$$

for n > 1:

$$dC_n/dt = k_3[C_n^*]$$

$$d[C_n^*]/dt = k_2[C_{n-1}^*][A] - (k_2[A] + k_3)[C_n^*] \qquad (5.3)$$

where $k_2 = k_2^o$ when $C_1^{**} = A$
$k_2 = k_2^o K$ when $[C_1^{**}] = K[A]$

- For the condensation model, and the polymerization model (where $C_1^{**} = C_1^*$ or $[C_1^{**}] = K[C_1^*]$)

$$dC_1/dt = k_1[C_1^*]$$

$$d[C_1^*]/dt = k_+[A] - (\sum_{n=1}^{\infty} k_2[C_n^*] + k_1 + k_-)[C_1^*] \qquad (5.4)$$

for n > 1:

$$dC_n/dt = k_3[C_n^*]$$

$$d[C_n^*]/dt = k_2[C_{n-1}^*][C_1^*] - (k_2[C_1^*] + k_3)[C_n^*] \qquad (5.5)$$

where $k_2 = k_2^o$ when $C_1^{**} = C_1^*$
$k_2 = k_2^o K$ when $[C_1^{**}] = K[C_1^*]$

For the formation of the initiation species C_1^*, two extremes are possible. Either its formation is, or is not the rate determining step. When the initiation is rate determining $k_- C_1^*$ will approach to zero in equations 5.2 and 5.3.

To be able to calculate the production rate of hydrocarbons as a function of time, an assumption has to be made with respect to the surface coverage of carbon containing intermediates. Dautzenberg et al. proposed two extremes with respect to the surface coverage of A. In the first extreme the intermediate A is only formed at the start of the CO/H_2-pulse, covering all available sites. A is converted to hydrocarbon surface intermediates and no additional A is formed. In the second proposal the concentration of A is constant throughout the time of the pulse. In their first concept, the rate of hydrocarbon formation will decay to zero. Their second approximation can only be valid for low surface coverages of hydrocarbon intermediates.

In our study we assume that during the pulse the *total* surface coverage of carbon containing intermediates is constant in time and that carbon species cover almost the entire surface.

Both the propagation and the termination reaction will require a certain amount of hydrogen. In principle the coverage of hydrogen will be a function of the surface coverage of carbon containing species and the pressure of hydrogen, hence

$$[H] = f\left(\sum_{n=1}^{\infty} [C_n^*] + [A] + [C_1^{**}], p_{H_2}\right)$$

Because it is assumed that the surface coverage of carbon containing species is independent of time, the same applies to the coverage of hydrogen at constant hydrogen partial pressure. Hence

$$k_2' [H]^m = k_2'' p_{H_2}{}^{m/2} = k_2$$

and

$$k_3' [H]^n = k_3'' p_{H_2}{}^{n/2} = k_3$$

In the case of a steady state production, the coverages of hydrocarbon intermediates with $n \geq 1$ are related to the surface coverage of C_1^* by:

$$[C_n^*(\infty)] = \alpha^{n-1} [C_1^*(\infty)] \tag{5.6}$$

The total surface coverage of hydrocarbon intermediates can be expressed as:

$$\sum_{n=1}^{\infty} [C_n^*(\infty)] = \frac{1}{1-\alpha} [C_1^*(\infty)] \tag{5.7}$$

When we apply equation 5.7 to the data of Dautzenberg et al., i.e. $\alpha = 0.95$ and $C_1^*(\infty) = 0.13$ we obtain for the total degree of coverage $\sum_{n=1}^{\infty} [C_n^*(\infty)] = 2.6$, whereas the authors report $\sum_{n=1}^{\infty} [C_n^*(\infty)] = 0.7$.

If it is assumed that the rate constants of propagation and termination do not change during the synthesis, it is possible to express k_2^o and k_3 as a function of the turnover frequency for CO-conversion to hydrocarbons (N_{CO}), the turnover frequency for CH_4-formation (N_{CH_4}), the probability of chain growth (α), the steady state coverage of the precursor A and the value of the equilibrium constant K. This is done by applying the assumption that the surface is almost entirely covered with carbon containing species, hence

	MODEL			
	Condensation/ polymerization $(C_1^{**} = C_1^*)$	Polymerization $([C_1^{**}] = K[C_1^*])$	CO-insertion/ polymerization $(C_1^{**} = A)$	CO-insertion $([C_1^{**}] = K[A])$
k_2^o	$\frac{N_{CO}-N_{CH_4}}{(1-[A(\infty)])^2(1-\alpha)(2-\alpha)}$	$\frac{N_{CO}-N_{CH_4}}{K(1-[A(\infty)])^2(1-\alpha)(2-\alpha)}(1+K(1-\alpha))^2$	$\frac{N_{CO}-N_{CH_4}}{[A(\infty)](1-[A(\infty)])(2-\alpha)}$	$\frac{N_{CO}-N_{CH_4}}{K[A(\infty)](1-(1+K)[A(\infty)])(2-\alpha)}$
k_3	$\frac{N_{CO}-N_{CH_4}}{(1-[A(\infty)])\alpha(2-\alpha)}(1-\alpha)$	$\frac{N_{CO}-N_{CH_4}}{(1-[A(\infty)])\alpha(2-\alpha)}(1+K(1-\alpha))(1-\alpha)$	$\frac{N_{CO}-N_{CH_4}}{(1-[A(\infty)])\alpha(2-\alpha)}(1-\alpha)$	$\frac{N_{CO}-N_{CH_4}}{(1-(1+K)[A(\infty)])\alpha(2-\alpha)}(1-\alpha)$

Table 5.1. The reaction rate constants for propagation and termination expressed as a function of turnover frequencies, probability of chain growth, steady state surface coverage of the precursor A en the equilibrium constant K.

$\sum_{n=1}^{\infty} [C_n^*] + [C_1^{**}] + [A] \sim 1$. The constant k_2^o is then derived by substituting equation 5.7 in the steady state form of equation 5.2 and 5.4. The turnover frequencies can be expressed as $N_{CO} = k_+[A] - k_-[C_1^*]$, and $N_{CH_4} = k_1[C_1^*]$. The reaction rate constant for termination is calculated by substituting the expression found for k_2^o in equation 5.1. The resulting expressions are given in table 5.1.

Dautzenberg et al. claim low rate constants for the propagation reaction. With the rate constant (k_2^o) shown in table 5.1, it is possible to calculate the rate constant of propagation for the case where the rate of the reaction is completely determined by this constant. This is done by minimization of the k_2^o with respect to K and $[A(\infty)]$. The minimal values of k_2^o are shown in table 5.2. The first three constants reported are straightforward minimizations. The minimal value of k_2^o for CO-insertion ($[C_1^{**}] = K[A]$) would be obtained mathematically when $[CO] = 0.5$ and $[A] \to 0$, but this is thermodynamically not feasible ($[CO]$ must be smaller or equal to $[A]$). Therefore the minimum value for k_2^o appears for $[CO] = [A] = 0.25$.

	MODEL			
	Condensation/ polymerization ($C_1^{**} = C_1^*$)	Polymerization ($[C_1^{**}] = K[C_1^*]$)	CO-insertion/ polymerization ($C_1^{**} = A$)	CO-insertion ($[C_1^{**}] = K[A]$)
minimum value for k_2^o appears when:	$[A(\infty)] \to 0$	$[A(\infty)] \to 0$ $K = \frac{1}{1-\alpha}$	$[A(\infty)] = 0.5$	$[A(\infty)] = 0.25$ $K = 1$
k_2^o	$\frac{N_{CO}-N_{CH_4}}{(1-\alpha)(2-\alpha)}$	$\frac{N_{CO}-N_{CH_4}}{0.25(2-\alpha)}$	$\frac{N_{CO}-N_{CH_4}}{0.25(2-\alpha)}$	$\frac{N_{CO}-N_{CH_4}}{0.125(2-\alpha)}$

Table 5.2. Minimal reaction rate constants for propagation derived from the k_2^o values shown in table 5.1.

With the rate constants shown in table 5.2, and the values for N_{CO}, N_{CH_4} and α reported in the literature, it is possible to calculate the minimum rate constant for propagation that will fit the catalyst performance when the rate is determined by propagation. The

values for the rate constant k_2^o on ruthenium are calculated from the data published by Dautzenberg et al.[3], for the propagation rate constants on iron the data of Vannice are used[2]. For the case of ruthenium, it is assumed that the methame production meets the Schulz-Flory distribution ($k_1 = k_3$). The values for the minimal rate constants of propagation are shown in table 5.3.

	MODEL			
	Condensation/ polymerization ($C_1^{**} = C_1^*$)	Polymerization ($[C_1^{**}] = K[C_1^*]$)	CO-insertion/ polymerization ($C_1^{**} = A$)	CO-insertion ($[C_1^{**}] = K[A]$)
k_2^o for Ru (s^{-1})	3.0×10^{-1}	6.1×10^{-2}	6.1×10^{-2}	1.2×10^{-1}
Data for Ru: $N_{CO} = 1.6 \times 10^{-2}$ (s^{-1}); $N_{CH_4} = 4.0 \times 10^{-5}$ (s^{-1}); $\alpha = 0.95$				
Definition k_2 used by (3) $k_2 = k_2^o[C_1^{**}]$ → reported value $k_2 = 1.6 \times 10^{-2}$ (s^{-1})				
Calculated k_2^o from table 5.2 (s^{-1})	1.5×10^{-2}	3.1×10^{-2}	3.1×10^{-2}	3.0×10^{-2}
k_2^o for Fe (s^{-1})	1.6×10^{-1}	2.9×10^{-1}	2.9×10^{-1}	5.7×10^{-1}
Data for Fe: $N_{CO} = 1.6 \times 10^{-1}$ (s^{-1}); $N_{CH_4} = 5.7 \times 10^{-2}$ (s^{-1}); $\alpha = 0.56$				

Table 5.3. Minimal numerical values for the reaction rate constants for propagation. The values are derived by substitution of the data reported by Dautzenberg et al.[3] for ruthenium, and by Vannice[2] for iron in the expressions shown in table 5.2.

By comparison of the value for k_2 reported by Dautzenberg et al. and the values calculated for the different models, it can be concluded that for ruthenium the reaction rate is completely determined

Figure 5.1. Simulation of the transient response of iron catalysts to the introduction of synthesis gas to the reactor, when the propagation step is rate limiting. The data required for the simulation are taken from the work of Vannice[2]. Reaction temperature 550 K; CO/H_2 = 0.33; pressure 0.1 MPa.

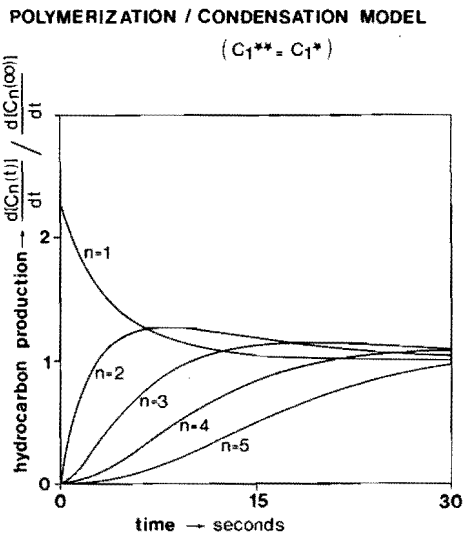

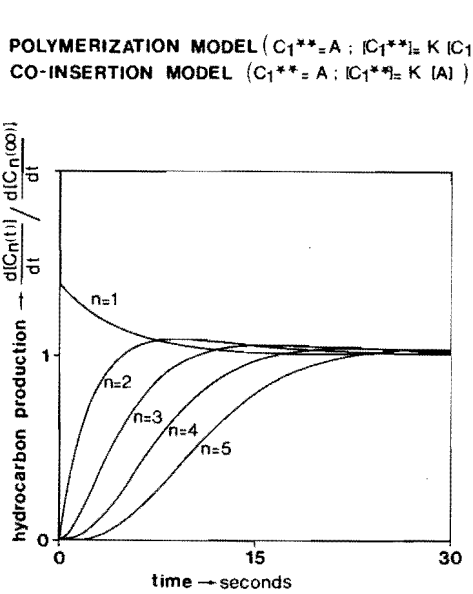

by the rate of propagation. When it is assumed that the same is applicable in the case of iron it is possible to simulate the non steady state behavior of the iron catalyst using the data of Vannice. The simulation for the different models was performed by numerical integration of the rate equations 5.3 and 5.5. The Continuous System Modeling Program for the B6700 (CSMP73) was used to solve the integrations. A number of assumptions are made with respect to the initial conditions:

- as is already discussed, the carbon containing species cover almost the entire surface. This coverage is constant in time;
- the second assumption is that instantly equilibrium is obtained between A, C_1^* and C_1^{**};
- the last and most essential assumption is that the activity of the catalyst is constant in time.

The simulated dimensionless rates of hydrocarbon evolution as a function of time is depicted in figure 5.1. The rate constants k_2^o for iron as shown in table 5.3 (column 5) are used for this simulation. The rates in figure 5.1 reflect the deviation of the hydrocarbon production from steady state. These results now can be used to cheque experimentally whether the assumption of a limiting propagation rate fits the data.

5.3. EXPERIMENTAL

5.3.1. The catalyst

A catalyst with a low sulphate content (approximately 0.006 wt % $Fe_2(SO_4)_3$) is used in the transient experiments. Prior to the experiments, 0.27 g reduced catalyst is activated in continuous stream of synthesis gas ($x_{CO} = x_{H_2} = 0.2$). The diameter of the catalyst pellets ranges from 0.175 to 0.2 mm.

5.3.2. Apparatus

The experiments are performed in the pulse reactor system described in chapter 2 (system IV).

5.3.3. *Analysis*

The reactants and products are analysed with a Finnigan 4000 quadrupole mass spectrometer. Via a capillary the outlet of the reactor is connected to the ionisation chamber of the mass spectrometer.

5.3.4. *Procedure*

After the catalyst has reached a steady state synthesis activity the synthesis gas stream is switched to a hydrogen/helium gas mixture (ratio 0.25) at a velocity of 0.75 cm^3/s and 0.25 MPa. The temperature in the reactor is held at 550 K. When the production of hydrocarbons is very small, the H_2/He stream is replaced by synthesis gas for 20 seconds, whereafter again H_2/He is fed to the catalyst. Pressure, temperature and feed are carefully held constant during this treatment. A second experiment is carried out that is almost identical to the one described above. The only difference is that instead of a mixture of hydrogen and helium, pure helium is used in the periods between the introduction of synthesis gas.

5.4. *RESULTS AND DISCUSSION*

Different types of carbon are formed during the synthesis on iron catalysts. These species have been characterized with respect to their reactivity towards hydrogen in the former chapter. The most reactive species towards hydrogen, that is referred to as α'-carbon, is thought to be the active species. This active species can react to hydrocarbon intermediates on the surface, which in their turn can react to hydrocarbons. To be able to determine the transient behavior of the iron catalyst conform the kinetic treatment described in paragraph 5.2, hydrocarbon intermediates are allowed to be present on the catalyst surface at the start of the experiment. On the other hand, because carbided iron is the active catalyst in the synthesis, the carbide structures have to be present as completely as possible. For this reason, the catalyst is activated in a continuous stream of synthesis gas at 550 K until a steady state hydrocarbon production is obtained, prior to the transient experiment. The surface carbon

Figure 5.2. Transient response to a 20 second block pulse of synthesis gas in hydrogen of a Fe/ZnO catalyst at 550 K and 0.25 MPa ($x_{H_2} = x_{CO} = 0.2$).

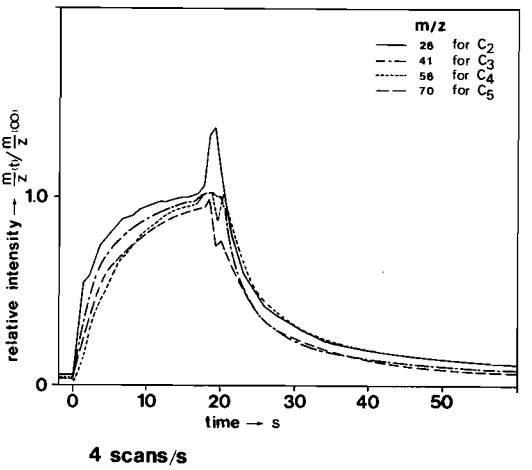

containing species are then removed by a continuous stream of H_2/He (ratio 0.25) over the catalyst bed at 550 K. The hydrocarbon production of this flushing treatment is constantly monitored with the mass spectrometer. When the hydrocarbon production is negligible, synthesis gas is fed to the catalyst for 20 seconds. After this period the H_2/He gas stream is again restored. Because the methane formed from hydrogenation of carbide structures interfered with the methane produced from the hydrogenation of surface carbon species, the methane production does not render first-hand information with respect to the kinetics of the Fischer-Tropsch synthesis. Therefore only C_2 to C_5 hydrocarbons are analysed during the 20 second exposure of synthesis gas to the catalyst. In figure 5.2, the most appropriate m/z-values for C_2-C_5 hydrocarbons are depicted as a function of time. In this figure the intensity of the signal is divided by its extrapolated steady state value, and thus is directly comparable to the simulated hydrocarbon evolution as shown in figure 5.1. By comparing figure 5.2 and 5.1, it can be seen that the rate of propagation cannot be the rate determining step on iron catalysts. There is hardly a difference in time between the evolution of C_2 and C_5 hydrocarbons, and no point of inflection appears in the evolution of the higher hydrocarbons. When the surface carbon species are not reduced

by hydrogen prior to the introduction of synthesis gas, the steady state hydrocarbon production is obtained more rapidly. This is shown in figure 5.3, where the experiment described above is repeated with pure helium as a carrier gas. The difference between figures 5.2 and 5.3 can be explained by a not fully carbided, hence not fully active, surface at the start of the experiment when H_2/He is used as a carrier gas.

Figure 5.3. Transient response of a Fe/ZnO catalyst to a 20 second block pulse of synthesis gas in helium at 550 K and 0.25 MPa ($x_{H_2} = x_{CO} = 0.2$).

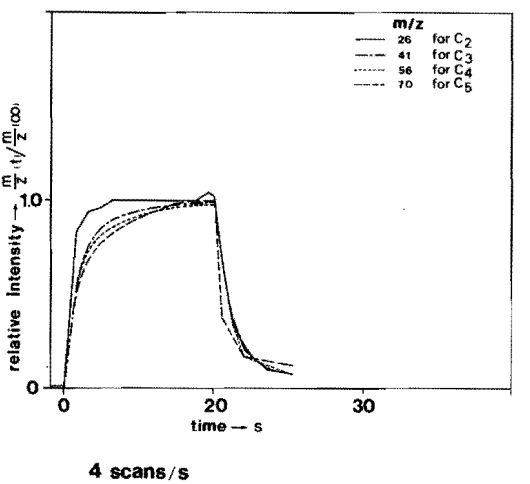

5.5. *CONCLUSIONS*

A comparison of a theoretical treatment of the rate of synthesis of hydrocarbons with the experimental results, clearly shows that the rate of the synthesis reactions on iron is not determined by the rate of propagation. This result is in contrast with the conclusion of Dautzenberg et al. for ruthenium. This does not signify, however, that the propagation of ruthenium has to be rate determining. There are a number of indications in the literature that the assumptions made by Dautzenberg et al. may not be fulfilled during their experiments. Firstly, the authors assume that the intrinsic activity of the catalyst does not change during the synthesis. However, on ruthenium,

which in this case shows a behavior comparable to iron, the catalyst is slowly activated when introduced to synthesis gas. The activation is accompanied by changes in the selectivity. Ponec et al.[4] attribute these changes in the behavior of ruthenium to the deposition of carbon, and not to the low intrinsic activity of the catalyst to propagation. Furthermore, Madon[5] showed that the simple Flory-Schulz distribution does not apply to a Ru/Al_2O_3 catalyst, while the application of the Schulz-Flory distribution is an essential part of the treatment of Dautzenberg and coworkers.

REFERENCES

1. Burwell, R.L., Pure and Appl. Chem. 46, 71 (1976)
2. Vannice, M.A., J. Catal. 37, 449 (1975)
3. Dautzenberg, F.M., Helle, J.N., van Santen, R.A., Verbeek, H., J. Catal. 50, 8 (1977)
4. Ponec, V., van Barneveld, W.A., Ind. Eng. Chem. Prod.-Res. Dev. 18, 2, 268 (1979)
5. Madon, R.J., J. Catal. 57, 183 (1979)

CHAPTER 6

Final discussion

6.1. INTRODUCTION

In this last chapter an attempt is made to explain the behavior of the iron catalyst in the Fischer-Tropsch synthesis, using data from the literature and the results presented in the foregoing chapters.

In the chapters presented so far, the activity and selectivity of the catalyst have played an important role, not in the least because these aspects determine the viability of the process under study to a large extent.

Active site and turnover frequency are concepts directly related to activity. Some considerations with respect to these concepts will be given at the end of this chapter.

6.2. ACTIVITY AND SELECTIVITY

In general, the activity of a catalyst is not only a function of the amount of active sites, but also of the intrinsic activity of these sites. From the literature it is not clear whether the low activity of Fischer-Tropsch catalysts is due to a small number of active sites or to sites of a low activity. Rautavuoma[1] states that the low activity of cobalt catalysts is due to a small amount of active sites. On the other hand, Dautzenberg et al.[2] find that the intrinsic activity of the sites on ruthenium is low.

Whatever factor may be responsible for the low activity of iron catalysts, we do know that iron in its metallic form is inactive in the synthesis. Under process conditions the catalyst gradually activates, whereby the catalyst is converted to iron carbide. In chapter 4 it is shown that a species that is likely to be the active species in the synthesis (α'-carbon) is formed on the surface when the toplayers of the catalyst are reconstructed. The same carbonaceous species are formed during the carbidisation of the catalyst, and it is probable that the reconstruction is brought about by the carbidisation. If we go one step further in our argumentation, it can be said that active sites are created by the carbidisation, or that the extent of carbidisation of the catalyst determines the amount of active sites on the catalyst.

In chapter 4, the deactivation of the catalyst is ascribed to the formation of a carbon layer over the active iron carbide surface. This explanation has originally been proposed by Dwyer[3]. However, there are a number of publications that points to an alternative explanation of the deactivation[4,5]. According to the publication of Pichler et al.[4], two structures of the catalyst are inactive. At the one end, a metallic iron catalyst is inactive and, on the other end, a fully carbided catalyst neither shows activity. Hence, only a partly carbided iron surface is active in the synthesis. Pichler et al. express this view by stating that a small but important part of the catalyst must expose free iron. Adsorption measurements on iron samples[5] show that most of the capacity for carbon monoxide as well as for low-temperature hydrogen adsorption is eliminated when the catalysts are carburized. Although it is not possible to differentiate between the two deactivation models on basis of experimental results, the latter model can also explain qualitatively the changes in selectivity that are noticed during the carbidisation.

Apart from the changes in the activity of the catalyst, also selectivity changes are observed during the carbidisation. In chapter 3, it is found that by increasing the temperature from 525 K to 625 K, the olefine-to-paraffine ratio increases. This change in selectivity cannot be ascribed to the effect of the temperature on the residence time of olefine molecules at the surface, for a decrease in the temperature has no influence on the olefine-to-paraffine ratio after the catalyst was previously brought at a steady state at 625 K. Hence,

the characteristics of the catalyst did change when the synthesis temperature was raised from 525 K to 625 K. This aspect of selectivity may be explained by a reduced affinity of the catalyst towards hydrogen, because the surface of the catalyst is in a more carbided form at the higher temperature. A second possibility is that the reduced carbon-to-metal bondstrength upon carbidisation facilitates the desorption of the olefinic product thereby reducing the secondary reaction of hydrogenation of olefines to paraffines. One would expect that a catalyst with a low hydrogenation activity would also show a low methane selectivity, as would agree with the experiments of Rautavuoma[1] (figure 1.1 curve c). However, the iron catalyst displays a methane production at 625 K that does not deviate from the Schulz-Flory distribution (figure 3.3 curve b). The isothermal hydrogenation experiments described in chapter 4 show that only the active species (α'-carbon) give an appreciable amount of higher products upon hydrogenation (figure 4.3). Hence, the high methane selectivity of the iron catalyst obtained at 625 K, can be explained by a large contribution of methane formed from hydrogenation of carbides and/or of deactivating surface carbon (figure 4.5).

Summarizing, the foregoing speculative model says that both the amount and the selectivity of the active sites are determined by the carbide content of the surface. A strongly carburized catalyst surface is obtained at high synthesis temperatures, reducing the hydrogenation activity of the catalyst. Correspondingly, the catalyst has a low activity and the olefine-to-paraffine ratio is high at more elevated temperature.

With this model, in which the carbide content of the catalyst surface determines both the activity and the selectivity of the catalyst, it is possible to explain the sulphur promoting effect. Van Dijk et al.[6] proved that carbon deposits on nickel catalysts reduce the quantity of strongly adsorbed carbon monoxide. The same observations have been found on ruthenium by Dalla Betta[7]. Upon sulphur poisoning an effect similar to that of carbon deposition is noticed on nickel[8] and on iron[9]. For this reason Ponec[10] states that sulphur can be regarded as a substitute for carbon. The results presented in chapter 3 show that sulphur promotion reduces the carbidisation ability of the iron catalyst and decreases the carbon monoxide adsorption capacity. With respect to the hydrogenation activity the effect of

sulphur also resembles that of carbon. It is shown in chapter 4 (figure 4.13), that by adding sulphur to the iron catalyst, the hydrogenation ability is reduced. From the foregoing it can be concluded that at a synthesis temperature of 625 K the sulphur-promoted catalyst surface can be considered as being less carburized when compared to the unpromoted iron surface. The less carburized sulphur-containing surface has the same low hydrogenation activity as the heavily carburized unpromoted surface, but it does not show the high methane selectivity of the unpromoted catalyst.

The discussion about the role of the carbide in the activity of the iron catalyst has been started with the statement that the extent of carbidisation determines the amount of active sites. At this point in the discussion we want to mention that the extent of carbidisation is also likely to influence the intrinsic activity of the sites by changing the affinity of the catalyst towards the reactant gases. The question whether the low activity of the catalyst is determined by the small number of active sites or the low intrinsic activity of these sites still needs to be discussed. We already explained in the introduction of chapter 5, that the amount of CO adsorbed on the reduced iron catalyst is an ambiguous measure for the amount of active sites. If we would be able to determine the amount of active carbon species on the surface this would be a more reliable characteristic. From the amount of α'-carbon species (figure 4.6) present on the surface of the active catalyst, a turnover frequency of $N_{CH_4} = 0.004\ s^{-1}$ is calculated. This value is of the same order of magnitude as the turnover frequency published by Vannice[11] after correction for the pressure difference ($N_{CH_4} = 0.009\ s^{-1}$ at 550 K; 100 kPa; $x_{H_2} = x_{CO} = 0.2$). This low turnover frequency could agree with the low rate constant of propagation that has been reported by Dautzenberg et al.[2]. From the results presented in chapter 5, it is concluded that on iron catalysts the propagation is not rate-determining. This does not imply that the intrinsic activity of the sites has to be higher than the value that would follow from the turnover frequency. In chapter 5 the results are based on transient response measurements. Other reaction steps that give no transient response may determine the low activity of the active sites.

At this point it may be useful to discuss the type of reaction mechanisms that could show transient response and, in some more detail, the concept of turnover frequency and the related expression active site.

6.3. TURNOVER FREQUENCY AND ACTIVE SITE

The concepts turnover frequency and active site are in some way related to the rate-determining step of the reaction. In the idealized concept of the rate-determining step (RDS) of irreversible reactions, all elementary steps preceding the RDS are supposed to be in rapid equilibrium, and all steps after the RDS fast and irreversible. In the transient state theory an equilibrium is assumed between the reactants (including the active sites) and the activated complex. In this concept a catalyst exhibiting adsorption-desorption equilibrium will establish a steady state concentration of activated complexes very fast. These activated complexes will have a constant chance to be converted to the product. In this context, the chance should be interpreted as the chance of each activated complex to be converted in the next second. If we denote this chance by p (s^{-1}) and the number of activated complexes by n (moles/kg cat), then the rate of the RDS is:

$$r_R = p \cdot n_a$$

This rate will be constant as soon as n_a is constant. Thus in case the steady state concentration of activated complex is reached very fast, no transient behavior will be noticed, and steady state conversion is reached as from the beginning of the experiment. Only when in the reaction sequence steps occur at a rate of the same order of magnitude as the RDS, the steady state concentration of activation complexes n_a will be established with a marked rate. A number of possibilities can be brought forward in this context.

- The rate of desorption of one of the products is comparable to the rate of the RDS, thus decreasing the number of sites available for reaction. An example of transient response due to the slow desorption of the product is offered by Kobayashi and Kobayashi[12]. The

authors have studied the decomposition of nitrous oxide on MnO, and noticed that the decomposition initially occurs at a much higher rate than at steady state. This phenomenon can be explained by coverage of part of the surface by oxygen due to the slow desorption of oxygen.

- The rate of reaction is not determined by one RDS but by a consecutive series of steps, all with comparable rates. An example of this possibility is described in chapter 5 for the Fischer-Tropsch synthesis, when the rate is determined by the rate of propagation (figure 5.1).
- The formation of the reactants for the RDS induce heterogeneities in the distribution of the reactants on the surface, and the rate of surface migration of the reactants is of the same order as the rate of the RDS. This could for example occur if we assume that the RDS in the Fischer-Tropsch synthesis is the formation of CH_2^* species, formed by hydrogenation of C* as expressed in reaction 2 in the mechanism shown below.

Reaction mechanism for the Fischer-Tropsch synthesis

$$CO^* + * = C^* + O^* \quad (1)$$

or

$$C^* + 2\,H^* = CH_2^* + 2\,* \quad (2)$$

$$CH_2^* + C_jH_{2j}^* = C_{j+1}H_{2j+2}^* + 2\,* \quad (3)$$

$$C_jH_{2j}^* + 2\,H^* = C_jH_{2j+2} + 3\,* \quad (4)$$

$$C_jH_{2j}^* = C_jH_{2j} + * \quad (5)$$

It is possible that initially after the formation of C* there is a low chance that C* species will be hydrogenated because the H* concentration in the neighbourhood of C* is temporarily low, for the prefered reduction of the O* species formed in reaction 1 consumes H* species from the vicinity. No equilibrium between reactants and the activated complex is attained here.

- The formation of the reactants that are required in the RDS takes place at a site that is not the same as the site required for the RDS, and the rate of surface diffusion of the reactants is of the same order as that of the RDS.

In the remainder of the discussion we will focus our attention on the concept of turnover frequency. The degree of advancement of a single catalytic reaction is measured by the rate defined as:

$$r = (1/Q)\ (dS/dt)$$

where S is a parameter expressed in moles, t is the time and Q is the mass or the surface area of the catalyst.
For the clarity of the discussion, we introduce the *overall* turnover frequency (N) which is related to an alternative value of Q, viz. the total number of moles of surface sites. Hence, N is defined as the number of moles reacting per mole of surface sites per second. This N gives an upper value for the value of the *true* turnover frequency (N_T), defined according to the IUPAC definition[13] (see introduction chapter 5), that is based on the population of the catalytically active sites, the number of which may be only a fraction of the total number of surface sites. It must be emphasized that according to the definition the value of N_T is determined by the sum of the number of empty active sites and of active sites occupied by reactants. The inverse of the turnover frequency is not a measure for the mean reaction time per elemental conversion (which is the reciproque of the reaction rate constant), but is the mean reaction time per elemental conversion divided by the fraction of active sites covered with the reactants in the rate-determining step. In our opinion, the concept of active site may have to be enlarged. Lankhuijzen[14] has distinguished the following surface elements:
- active site;
- active centre;
- active ensemble;
- active aggregate.

For the Fischer-Tropsch synthesis we can conceive *active sites* for the adsorption of hydrogen atoms, presumably *active centres* for the adsorption of double bonded species like $CH_2<$ or CO<, and *active ensembles* for each of the reaction steps as presented in the reaction

mechanism for the synthesis. Whereas the number of active sites (empty plus occupied) (n_s), is in principle a simple countable quantity, the number of active centres (n_c) and active ensembles (n_e) has partly a statistical meaning as the total number of these species is determined by the combinations formed. If a number of a sites form an active centre or an active ensemble, then

$$n_c < n_s/a \text{ and } n_e < n_s/a$$

Further it may well be possible that not all the sites counted in n_s can partake in the formation of active centres or ensembles. It is also possible that the active ensembles for e.g. reactions 2 and 3 of the presented reaction mechanism have different locations on the catalyst, and that the species taking part in reaction 2 have to be transported from the site or centre on which they are adsorbed after formation to the location of the ensemble required for reaction 3. The total of the active sites centres and ensembles required to make a product from the reactant gases will form one *active aggregate*. One of the topics that is frequently discussed in the literature lately, is the number of sites of the active ensemble needed for the Fischer-Tropsch reaction. The values reported recently do not agree with each other. Dalmon et al.[15] find that for the formation of methane 12 sites are required, and for the production of higher hydrocarbons 20, while Luyten et al.[16] claim that only 4 or 5 sites are needed. The type of nomenclature presented here may contribute to a discussion about what is really meant by the amount of active sites needed for the Fischer-Tropsch reaction.

REFERENCES

1. Rautavuoma, A.O.I.. Thesis, TH Eindhoven (1979)
2. Dautzenberg, F.M., Helle, J.N., van Santen, R.A., Verbeek, H., J. Catal. 50, 8 (1977)
3. Dwyer, D.J., Somorjai, G.A., J. Catal. 52, 291 (1978)
4. Pichler, H., Schulz, H., Chem.-Ing.-Techn. 42, (18) (1970)
5. Podgurski, H.H., Kummer, J.T., Witt, T.W., Emmett, P.H., J. Am. Chem. Soc. 72, 5382 (1950)

6. Van Dijk, W.L., Groenewegen, J.A., Ponec, V., J. Catal. 45, 277 (1976)
7. Dalla Betta, R.A., Shelef, M., J. Catal. 48, 111 (1977)
8. Rewich, R.T., Wise, H., J. Phys. Chem. 82, 751 (1978)
9. Rhodin, T.N., Brucker, C.F., Solid State Comm. 23, 275 (1977)
10. Ponec, V., Catal. Rev.-Sci. Eng. 18, (1), 151 (1978)
11. Vannice, M.A., J. Catal. 37, 449 (1975)
12. Kobayashi, H., Kobayashi, M., Catal. Rev.-Sci. Eng. 10, (2), 139 (1974)
13. Burwell, R.L., Pure and Appl. Chem. 46, 71 (1976)
14. Lankhuijzen, S.P., Thesis, TH Eindhoven (1979)
15. Dalmon, J.A., Martin, G.A., 7th Int. Cong. Cat., Tokio (1980)
16. Luyten, L.J.M., van Hooff, J.H.C., to be published

LIST OF SYMBOLS

C_1^*	initiating species for chaingrowth
C_1^{**}	building block for hydrocarbon chains
C_n^*	hydrocarbon surface intermediate with n carbon atoms
C_n	hydrocarbon product with n carbon atoms
C_o	carbon content of the catalyst (mol/g cat)
D	diameter of the catalyst bed (mm)
d_p	diameter of the catalyst pellets (mm)
E_a	activation energy (kJ/mol)
F	volumetric gas velocity (m^3/s) (N.T.P.)
k	reaction rate constant
K	equilibrium constant
L	length of the catalyst bed (mm)
m	mass of the analyzed ions
n	number of carbon atoms
n_a	number of activated complexes
n_c	number of active centres
n_e	number of active ensembles
n_s	number of active sites
N	overall turnover frequency (s^{-1})
N_T	turnover frequency (s^{-1})
N_{CH_4}	turnover frequency for methane formation (s^{-1})
N_{CO}	turnover frequency for CO-conversion to hydrocarbons (s^{-1})
p_Y	pressure of component Y in the gasphase (Pa)
r_Y	rate of formation or conversion of Y (mol/(s.g cat))
R	gas constant (kJ/(mol.K))
t	time (s)
T	temperature (K)
w_n	weight of the hydrocarbon product containing n carbon atoms (g)
w_o	weight of the total hydrocarbon product (g)

W	weight of the catalyst in its unreduced form (g cat)
x_y	mole fraction of component y in the feed
x'_y	weight fraction of component y in the catalyst
X	fraction of converted carbon
X_i	fraction of converted carbon at the maximum reaction rate
[Y]	fraction of the surface covered with species Y
(Y)	pressure of component Y in the gasphase (Pa)
z	charge of the analyzed ions
α	Schulz-Flory constant: $\alpha = \frac{r_{C_{n-1}}}{r_{C_n}}$

SUMMARY

When coal is gasified with steam to synthesis gas, which is a mixture of carbon monoxide and hydrogen, this gas can be converted to hydrocarbons via the Fischer-Tropsch synthesis. To obtain a profitable synthesis, the selectivity of the process has to be increased towards valuable products. We made it our object to obtain an attractive process by improving its selectivity towards the key petrochemical ethene.

With respect to the selectivity of the Fischer-Tropsch synthesis, the process conditions effect the composition of the product mix. However, it is not possible to obtain a profitable synthesis by only adopting the proper process conditions. The heterogeneous catalyst has to be modified to increase the selectivity to the desired level.

When compared to the product formed by other active metal catalysts, the product mix from iron catalysts approaches the required selectivity closest. For this reason iron is chosen as the active metal in the catalysts that are discussed in this thesis.

In differential plug-flow experiments it is found that the desired selective product mix is formed by high temperature synthesis over an iron catalyst that is doped with sulphate containing compounds prior to the reduction. A high synthesis temperature favours the production of shortchain hydrocarbons with a high olefine to paraffine ratio. The function of the sulphate ion in the catalyst is the selective suppression of the methane production rate. Apart from the change in the selectivity, sulphate doping of the catalyst also influences carbon deposition on the catalyst that determines the activity and life-time of the catalyst. From the two types of carbon that are formed during the synthesis, only one type lowers the hydrocarbon production rate by encapsulation of a part of the active surface. The formation of this type of carbon is partly inhibited by addition of small amounts of sulphate to the catalyst. The second type of carbon

causes desintegration of the catalyst pellet, which after long synthesis periods results in the plugging of the fixed-bed reactor. The formation of the latter type of carbon is only inhibited at relatively high sulphate concentrations in the catalyst. The disadvantage of using high sulphate concentrations is the low synthesis activity of the catalysts.

In order to get more information about the carbonaceous species that determine the synthesis performance of the catalyst, the species formed upon interaction of carbon monoxide and synthesis gas with the iron catalyst are studied. The temperature programmed surface reaction technique is used to distinguish between the different types of carbon. From this study it can be concluded that carbon monoxide adsorption on a freshly reduced catalyst results in the formation of carbonaceous species that are localized in sub-surface layers. The formation of these layers reconstructs the top atom layers of the catalyst. This reconstruction is maintained after the hydrogenation of the reconstructing carbonaceous species. When carbon monoxide is adsorbed on the reconstructed catalyst, species are formed on the catalyst surface that are most probably the active species in the synthesis.

In the second part of the study of carbonaceous deposits on the catalyst, different bulk-carbon species are identified with respect to their reactivity towards hydrogen. The hydrogenation of these bulk species during high temperature synthesis may well account for the high methane production of the unpromoted catalyst.

Finally, an attempt is made to discover whether the propagation step in the synthesis of hydrocarbons is as slow as is claimed in the literature. Because the formation of hydrocarbons can be described by a consecutive stepwise addition of mono-carbon units to a growing chain, a low propagation rate will give a transient evolution of hydrocarbons when the catalyst is introduced to synthesis gas. The type of response that would be expected for the case where the propagation is rate-determining is simulated. It is proven experimentally that the propagation rate is not rate-determining on iron catalysts. In a final discussion an attempt is made to explain the behavior of iron catalysts in the Fischer-Tropsch synthesis, and the attention is focused on the concept of turnover frequency and of the related expression 'active site'.

SAMENVATTING

Door steenkool te vergassen met stoom wordt synthesegas verkregen, een mengsel van koolmonoxide en waterstof. Dit gas kan door middel van de Fischer-Tropsch synthese worden omgezet in koolwaterstoffen. Voor een rendabele procesvoering is het nodig om de selectiviteit van de synthese voor de vorming van waardevolle produkten te verhogen. Om te komen tot een aantrekkelijk proces, is in ons laboratorium gekozen voor het verbeteren van de selectiviteit voor een van de belangrijkste grondstoffen voor de chemische industrie: etheen.

De condities waaronder de synthese wordt uitgevoerd alsmede de keuze van de katalysator hebben een belangrijke invloed op de samenstelling van het produkt. Het is echter niet mogelijk door optimale keuze van procescondities en door aanwending van bestaande katalysatoren te komen tot de vereiste selectiviteit. Een rendabel proces is slechts mogelijk bij toepassing van selectievere katalysatoren.

Het produkt dat wordt verkregen bij de synthese over ijzerkatalysatoren is wat betreft de selectiviteit voor etheen duidelijk superieur aan het produkt gevormd met andere metaalkatalysatoren. Om deze reden is gekozen voor de verbetering van katalysatoren waarin ijzer als aktief metaal optreedt.

In een differentiële propstroom reactor zijn verschillende ijzerkatalysatoren getest. Uit het onderzoek is gebleken dat de gewenste selectiviteit wordt bereikt door de synthese uit te voeren bij hoge temperatuur over een katalysator die is voorbehandeld met sulfaathoudende verbindingen. Door de keuze van een hoge synthesetemperatuur wordt een produkt gevormd dat vooral bestaat uit korte koolwaterstoffen met een hoge olefine/paraffine verhouding. De functie van het sulfaat in de ijzerkatalysator is de selectieve onderdrukking van de methaanproduktie. Afgezien van de invloed op de selectiviteit van de katalysator bepaalt sulfaat voor een belangrijk deel de afzetting van kool, die de activiteit en de levensduur van de katalysator bepalen.

Van de twee soorten kool die gedurende de synthese worden gevormd is één soort verantwoordelijk voor de daling van de synthese activiteit. Dit type kool, dat wordt afgezet op het oppervlak van de katalysator, kan voor een deel worden tegengegaan door toevoeging van kleine hoeveelheden sulfaatverbindingen aan de katalysator. De afzetting van een tweede type kool heeft tot gevolg dat de katalysatorkorrels verpoederen. Dit verpoederen is er de oorzaak van dat de vast-bed reactor na lange syntheseduur verstopt raakt. De vorming van dit laatste type kool wordt tegengegaan door een relatief grote hoeveelheid sulfaat aan de katalysator toe te voegen. Dergelijke hoeveelheden echter, verlagen de synthese activiteit van de katalysator.

Om nadere informatie te krijgen over de koolstofhoudende deeltjes die gevormd worden door interactie van de katalysator met koolmonoxide en synthesegas, en die van belang zijn voor de activiteit en selectiviteit van de katalysator, is een techniek gebruikt die temperatuur geprogrammeerde oppervlakte reductie wordt genoemd. Uit de studie met behulp van deze techniek komt naar voren dat bij de adsorptie van koolmonoxide op een vers gereduceerde katalysator, koolstofhoudende deeltjes worden gevormd die zich bevinden in lagen net onder het oppervlak. Bij de vorming van deze lagen vindt een hergroepering plaats van ijzeratomen dicht bij het oppervlak. De nieuwe configuratie van de ijzeratomen blijft behouden na hydrogenering van de koolstofhoudende deeltjes. Wordt na deze reductie opnieuw koolmonoxide geadsorbeerd, dan worden zeer reactieve koolstofhoudende deeltjes gevormd die naar aller waarschijnlijkheid de actieve intermediairen zijn in de synthese.

In een tweede deel van de studie van koolstofhoudende verbindingen op de ijzerkatalysatoren zijn verschillende bulkkoolstofverbindingen geïdentificeerd op grond van hun reactiviteit ten opzichte van waterstof. De hydrogenering van deze bulkverbindingen tijdens de synthese bij hoge temperatuur kan de oorzaak zijn van de hoge methaanproduktie van de niet met sulfaat gepromoteerde katalysatoren.

In het laatste experimentele deel van het proefschrift is nagegaan of in het mechanisme van de Fischer-Tropsch synthese de ketengroeistap zo langzaam is als in de literatuur wordt gemeld. In het geval van een lage propagatiesnelheid zal de snelheid waarmee de produkten worden gevormd vertraagd zijn ten opzichte van de snelheid waarmee de reactanten worden geïntroduceerd. Deze zogenaamde "transient response"

kan worden gebruikt om een indicatie te krijgen van de propagatie-snelheid, omdat de synthese kan worden beschreven als een stapsgewijze koppeling tussen enkelvoudige koolstofhoudende verbindingen en een groeiende keten. Een simulatie is gemaakt van het type response dat te verwachten is in het geval van een langzame propagatie. Het is experimenteel gebleken dat de propagatiestap snel moet zijn. In een laatste discussie wordt een verklaring gegeven voor het gedrag van ijzerkatalysatoren in de Fischer-Tropsch synthese, en wordt het belang van het concept "turnover-frequentie" en de hieraan verbonden term "actieve site" besproken.

LEVENSBERICHT

De schrijver van dit proefschrift werd op 2 september 1953 geboren te Arnhem. In 1971 behaalde hij het diploma H.B.S.-B op de Rijksscholengemeenschap te Wageningen. In datzelfde jaar begon hij zijn studie scheikunde aan de Rijksuniversiteit in Utrecht. Het kandidaatsexamen S1 (hoofdvak scheikunde; bijvakken natuurkunde en wiskunde) werd behaald op 3 november 1975. Het doctoraal examen (hoofdvak anorganische scheikunde, o.l.v. Prof.ir. J.W. Geus; bijvak fysische- en colloïdchemie, o.l.v. Prof.dr. G.A. Bootsma) werd met lof afgelegd op 30 januari 1978. Van 1 februari 1978 tot 1 maart 1981 was hij (in dienst van SON/ZWO) als wetenschappelijk assistent werkzaam bij de vakgroep Chemische Technologie van de Technische Hogeschool Eindhoven. Hier werd, in de groep van Prof.drs. H.S. van der Baan, het onderzoek uitgevoerd dat is beschreven in dit proefschrift.

DANKWOORD

Dit proefschrift is tot stand gekomen met medewerking van velen. In het bijzonder geldt dit voor de vakgroep Chemische Technologie. Aan al haar leden mijn hartelijke dank.

In het bijzonder dank ik de heer W.P.Th. Groenland, die met grote toewijding en kennis van zaken heeft meegewerkt aan het onderzoek.

De heer D. Francois en de heer R.J.M. van der Wey ben ik zeer erkentelijk voor de technische assistentie en de constructie-adviezen bij de opbouw van de vele reactorsystemen.

Verder ben ik dank verschuldigd aan de heer Ir. R.R. Poulina, die in zijn afstudeerperiode niet alleen heeft meegewerkt aan het in dit proefschrift beschreven onderzoek, maar ook door de vele discussies wezenlijk heeft bijgedragen aan mijn technologische ontwikkeling.

Aan de heer H.G. Eeuwhorst mijn dank voor de prettige samenwerking tijdens zijn keuzevakperiode in onze vakgroep.

Vele praktikanten en stagiaires dank ik voor de bijdrage die zij aan dit proefschrift hebben geleverd.

De vakgroep Instrumentele Analyse dank ik voor de gelegenheid die zij mij heeft geboden om experimenten uit te voeren met massaspectrometer analyse. In het bijzonder gaat mijn dank uit naar de heer Dr.ir. P.A. Leclercq en de heer G.J. Scherpenzeel die mij met raad en daad hebben bijgestaan bij het uitvoeren van de experimenten.

Mej. Dr. A.O.I. Rautavuoma en de heer Drs. W.L. van Dijk ben ik erkentelijk voor hun collegialiteit.

Ik dank de heer R.J.M. van der Wey die de tekeningen in dit proefschrift heeft verzorgd, de heer W.J.G. van Lith die zorg heeft gedragen voor de vormgeving van het omslag, mevr. C.E. Kieffer-Visser die het concept van het proefschrift op Engels taalgebruik heeft gecorrigeerd, en mevr. E.J.W.J. Eichhorn-Meijers die het vele typewerk en de lay-out van het proefschrift zoals gebruikelijk zeer punctueel heeft verricht.

ERRATA

page	line	states	read
7	3	a higher synthesis activity	it
17	12	on the effect of catalyst components	on the effect of changes in dispersion, pore structure, nature of interaction of catalyst components
19	9	selectivity	selectively
28	table 3.4	$p_{T,5}$, C_2H_5	$r_{T,5}$, C_2H_4
43	31	encapsulated	encapsulating
44	first formula	$\frac{1}{(1-\alpha)^2} C_n^*$	$\frac{1}{(1-\alpha)^2} C_1^*$
60	8	α' found	α' form
85	26	are allowed	are not allowed

STELLINGEN

1. Met de huidige kennis van het gedrag van zeolieten in de synthese van koolwaterstoffen uit methanol is het mogelijk te voorspellen welke zeolietstructuur een stabiele en selectieve katalysator voor de bereiding van korte olefinen zal opleveren. De vaardigheid om een dergelijke structuur ook te kunnen synthetiseren verdient een belangrijk onderzoeksdoel te zijn.

   Mobil Oil Corporation, U.S. Patent 4.079.095/096 (1978)

2. De toeneming van de selectiviteit voor de isomerisatie van glucose naar fructose onder invloed van hogere temperatuur, zoals Vellenga op grond van zijn model heeft aangenomen, wekt bij de koolhydraatchemicus op grond van zijn ervaring enige bevreemding.

   Vellenga, K., Proefschrift Rijksuniversiteit Groningen (1978)
   Pigman, W., Horton, D., The Carbohydrates, Acad. Press, 2nd ed., 165, N.Y. (1972)
   De Wilt, H.G.J., Proefschrift TH Eindhoven, 111 (1969)
   Beenackers, J.A.W.M., Proefschrift TH Eindhoven, 126 (1980)

3. Het argument dat bij pulsreactorexperimenten de conversie van een 0^{e}-ordereactie onafhankelijk kan zijn van de initiële concentratie, wordt door Hattori en Murakami ten onrechte betrokken bij de discussie over de relatie tussen conversie en pulsgrootte in geval van een 1^{e}-ordereactie.

   Hattori, T., Murakami, Y., J. Catal. 31, 127 (1973)

4. Kagan en Harrison nemen waar dat bij afzonderlijke injectie van twee isomeren op een gaschromatografisch systeem identieke 2-pieks chromatogrammen ontstaan. Hieraan verbinden de auteurs ten onrechte de conclusie dat thermische isomerisatie tijdens het transport door de kolom heeft moeten plaatsvinden.

Kagan, J., Harrison, D.A., Helv. Chim. Act. 55, 1728 (1972)

5. De overeenkomst tussen de Fischer-Tropsch-synthese van koolwaterstoffen en de Haber-synthese van ammoniak zoals deze is voorgesteld door Jones en Mc Nicol is vanuit kinetisch gezichtspunt aanvechtbaar.

Jones, A., Mc Nicol, B.D., J. Catal. 47, 384 (1977)

6. Het gebruik van het Michaelis-Menten-model door biochemici doet ten onrechte vermoeden dat het hier gaat om een andere kinetiek dan van het door chemici meer algemeen toegepaste Langmuir-Hinshelwood-model. Om een betere intradisciplinaire communicatie mogelijk te maken verdient het aanbeveling tot een meer uniforme modelbeschrijving te komen.

7. Ten onrechte hebben Pocker en Green op basis van literatuurgegevens bij de bestudering van de hydrolyse van D-gluconzuur-δ-lacton de vorming van het γ-lacton verwaarloosd.

Pocker, Y., Green, E., J. Am. Chem. Soc. 95, 113 (1973)
Michell, R.E., Duke, F.R., An. N.Y. Acad. Sci. 172, 129 (1970)
Levine, P.A., Simms, H.S., J. Biol. Chem. 68, 737 (1926)

8. De invoering van de Arbeidsomstandighedenwet ter vervanging van de Veiligheidswet maakt het eens te meer noodzakelijk in de opleiding van een chemisch ingenieur uitvoeriger aandacht te besteden aan de arbeidsveiligheidsaspecten van industriële activiteiten.

9. Naarmate men in de wetenschapsbeoefening meer gedetailleerde plannen voor de verre toekomst ontwikkelt, staat men des te steviger in de wetenschappelijke kinderschoenen.

Eindhoven, 17 maart 1981 E.Ph. Kieffer